Med Chem Res
DOI 10.1007/s00044-017-1858-1

MEDICINAL CHEMISTRY RESEARCH

ORIGINAL RESEARCH

Possible anticancer agents: synthesis, pharmacological activity, and molecular modeling studies on some 5-*N*-Substituted-2-*N*-(substituted benzenesulphonyl)-L(+)Glutamines

Tarun Jha[1] · Soumya Basu[1] · Amit Kumar Halder[1] · Nilanjan Adhikari[1] · Soma Samanta[1]

Received: 3 August 2015 / Accepted: 2 March 2017
© Springer Science+Business Media New York 2017

Abstract On the basis of our earlier work, fortyone 5-*N*-substituted-2*N*-(substituted benzenesulphonyl)-L(+)glutamines were synthesized and screened for cancer cell inhibitory activity. The best active compounds showed 91% tumor cell inhibition, whereas other three compounds showed more than 80% inhibition. Two-dimensional quantitative structure–activity relationship modeling and three-dimensional quantitative structure–activity relationship k-nearest neighbor molecular field analysis studies were done to get an insight into structural requirements toward further improved anticancer activity. Considering the fact that these compounds are competitive inhibitors of glutaminase, a molecular docking study followed by molecular dynamic simulation analysis were performed. The work may help to develop new anticancer agents.

Keywords Anticancer agent · Glutamine analog · 2D-QSAR · 3D-QSAR · Docking · MD simulation

Introduction

Due to the utilization in malignant cells both for an anaplerotic compound and for its reductive power (DeBerardinis et al. 2008a, b), glutamine is found to be a crucial nutrient for the rapidly growing cells (Newsholme et al. 2003; Turner and McGivan 2003; Martin et al. 1998; Wasa et al. 1996; Matsuno and Hirai 1989; Bhattacharya and Maity 2000). Glutamine plays an important role in tumor cell growth by supplying its amide nitrogen atom. It is observed in the biosynthesis of other amino acids, purine, pyrimidine, amino sugar and coenzymes (Zalkin and Smith 1998) with versatile mechanisms (Massiere and Badet-Denisot 1998). Glutamine provides multiple contributions by participating in protein, purine, and pyrimidine metabolisms. Almost one third of the circulating amino acids and nitrogen are transported by glutamine. It was also found to be a principal carrier of nitrogen from the skeletal muscles to the visceral organs (Klimberg and McClellan 1996). The levels of glutamine are undetectable in malignant strains of Earlich Ascite tumor cells (EATC) and ascite fluids (Marquez et al. 1989). Nevertheless, several reports revealed that glutamine transporter ASTC2 is overexpressed in gliomas, colorectal carcinoma, hepatoma, and neuroblastoma, and hence, a high glutamine uptake is found in different cancer cells (Huang et al. 2014; Xie et al. 2014; Hassanein et al. 2013; Ogura et al. 2011; Dolinska et al. 2003; Wasa et al. 2002; Witte et al. 2002). Moreover, glutamine is also found to modulate gene expression on different tissues. It triggers antiapoptotic Bcl-2 protein and helps to inhibit proapoptotic CD95 which, in turn, protecting these cells from apoptosis and thus, aids in malignancy (Chang et al. 2002). Furthermore, the higher level of glutamine catabolism by glutaminase enzyme has been proved to be a crucial feature of tumors in different origins.

Electronic supplementary material The online version of this article (doi:10.1007/s00044-017-1858-1) contains supplementary material, which is available to authorized users.

✉ Tarun Jha
tjupharm@yahoo.com

[1] Natural Science Laboratory, Division of Medicinal and Pharmaceutical Chemistry, Department of Pharmaceutical Technology, Jadavpur University, P.O. Box-17020, Kolkata 700032, India

Published online: 17 March 2017

During the exponential phase of cellular growth in several neoplasms, phosphate dependent kidney type glutaminase (KGA) activity was found to be the highest (Lu et al. 2010; Szeliga and Obara-Michlewska 2009). In rapidly proliferating cells of rat and human hepatomas, EATCs, human breast cancer cells and in human leukemias, KGA isoform is found to be highly overexpressed. Not only that, inhibition of KGA in EATCs activated apoptosis and sensitized these cells to hydrogen peroxide and methotrexate toxicity. Thus, inhibition of enzyme glutaminase is a potential target for anticancer therapy (Szeliga and Obara-Michlewska 2009). Therefore, it may be hypothesized that compounds which are able to reduce the uptake and utilization of glutamine and also may block or inhibit glutaminase in malignant cells, may elicit considerable anticancer potencies. In this article, we report some new 5-*N*-substituted-2-*N*-(substituted benzenesulphonyl)-L(+) glutamines as possible anticancer agents and also to explore theoretically the effect of these compounds on glutaminase enzyme. The general structure of 5-*N*-substituted-2-*N*-(substituted benzenesulphonyl)-L(+) glutamines is shown in Fig. 1.

This work is done as a part of our composite program of rational drug design and development (Adhikari et al. 2015; Kumar et al. 2015; Mondal et al. 2015; Das et al. 2015a, b; Hazra et al. 2015; Chatterjee et al. 2015; Chakraborty et al. 2015; Halder et al. 2015; Adhikari et al. 2014; Mondal et al. 2014; Chakraborty et al. 2014; Kumar et al. 2014; Chatterjee et al. 2014; Das et al. 2014; Adhikari et al. 2013a, b; Halder et al. 2013a, b; Mondal et al. 2013; Adhikari et al. 2012). The newly synthesized compounds were characterized and biologically evaluated by in vivo method considering the percent tumor cell inhibition (%TCI) as the biological activity parameter. To understand crucial structural and physicochemical factors responsible for the antitumor activities, two-dimensional quantitative structure–activity relationship (2D-QSAR) and three-dimensional quantitative structure–activity relationship (3D-QSAR) studies were performed. It was assumed that glutaminase is one of the targets of this series of compounds. Therefore, molecular docking and molecular dynamic simulation-based theoretical approaches were taken to understand the possible interactions of the best active compounds with the enzyme. In this attempt, the X-ray crystallographic structure of human glutaminase was docked with the best active compound and the ligand receptor interactions were reported. The stability of the docked ligand–receptor complex was analyzed by molecular dynamics (MD) simulation.

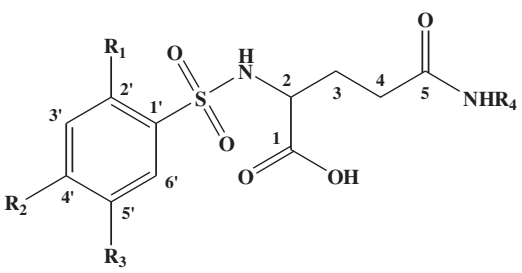

Fig. 1 General structure 5-*N*-substituted-2-*N*-(substituted benzenesulphonyl)-L(+) glutamines

Materials and methods

Chemistry

The preparations of the title compounds were carried out in four steps. The work started with the chlorosulphonylation of benzene derivatives **(1–7)** to obtain corresponding substituted benzenesulphonyl chlorides **(8–14)** (Huntress and Carten 1940). These benzenesulphonyl chlorides **(8–14)** were separately condensed with L(+) glutamic acid to get 2-N-(substituted benzenesulphonyl)–L(+) glutamic acids **(15–21)**. In this condensation, the reaction medium was maintained alkaline by 2 N NaOH solution so that the hydrochloric acid formed during the reaction was removed. Cyclization of the resulting diacids (**15–21**) with acetyl chloride produced 1-*N*-(substituted benzenesulphonyl)-5-oxopyrrolidine-2-carboxylic acids **(22–28)**. Aminolysis of these monoacids (**22–28**) with different amines resulted in the corresponding glutamine analogs (**29–69**). The route of synthesis is presented in Fig. 2.

Chemical characterization of all these compounds (**29–69**) was done by both analytical and spectrometric methods. Melting points of these compounds (**29–69**) were measured and verified by Mel-Temp Electrothermal apparatus-a capillary melting point apparatus and CTRONICS—a digital melting point apparatus. Structures of these synthesized final compounds were confirmed by infrared (IR)-, nuclear magnetic resonance (NMR)-, and mass spectroscopy as well as by the elemental analysis. All final compounds as well as L(+)-glutamic acid showed optical activity when observed in a polarimeter. IR spectra of these synthesized compounds (**29–69**) were recorded on SHIMADZU FTIR—8400 S Model by using KBr pellets. 1H NMR spectra were recorded at 25 °C in the pulsed Fourier Transformation mode on Bruker DRX 300 MHz NMR spectrometer. Chemical shifts are recorded in δ ppm (parts per million) in comparison with tetramethylsilane (Me4Si) as the internal standard for solutions in deuterated dimethylsulfoxide (DMSO-d6). Splitting patterns are represented as s (singlet), d (doublet) and m (multiplet). Positions of hydrogen described in 1H NMR interpretation are as per the general structure (Fig. 1) and substitutions at the R4 position are designated as the superscript "″" (double dash). All these reaction steps were monitored by the analytical

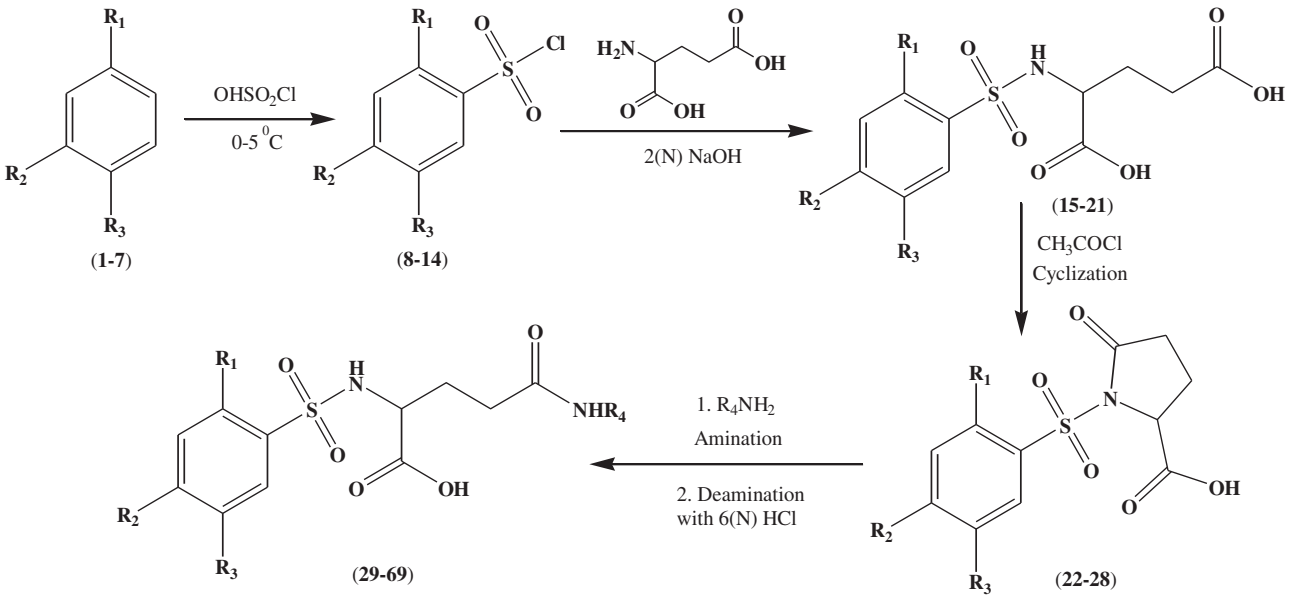

Fig. 2 General synthetic procedures of 5-*N*-substituted-2-*N*-(substituted benzenesulphonyl)-L(+) glutamines **(29–69)**

thin layer chromatography done on silica gel G plates. The spots were identified by keeping the thin layer chromtographic plates in iodine chamber.

Pharmacological activity

Biological evaluation of all these synthesized final compounds (**29–69**) was performed for their anticancer activities against Erlich ascites carcinoma (EAC) cells in Swiss Albino mice (Samanta et al. 2004). Female Swiss Albino mice of 10 weeks old with an average body weight of 18–20 g. were used for in vivo biological evaluation. Two groups of Swiss Albino mice each containing six healthy female mice (one test and the other control) were considered for the biological activity. All mice were kept in ambient room temp (20–27 °C) with basal metabolic diet and water ad libitum during these experiments. These final compounds (**29–69**) were dissolved separately into sterile phosphate buffer saline for the biological screening. Intraperitonially, these compounds (**29–69**) were administered individually after 24 h incubation of 2×10^6 EAC cells to each mouse. The total number of tumor cells was counted under a microscope with the help of a haemocytometer (Marienfeld, Germany). The mean of Ascites cells/ml was considered for evaluation of anticancer activity. The %TCI of these compounds (**29–69**) was determined individually. Mitomycin C, Azaserin, and DON in sterile phosphate buffers (pH 7.2) were utilized as standard drugs which showed 100% inhibitions. Mitomycin C was considered as the universal standard and azaserin as well as DON were chosen as the specific standard drugs to compare the activity of the test compounds.

Molecular modeling studies

The synthesized compounds were subjected to molecular modeling study by different methods such as 2D QSAR, k-nearest neighborhood-molecular field analysis (kNN-MFA) 3D QSAR, molecular docking and MD simulation analyses.

2D-QSAR study

2D-QSAR was performed on 41 synthesized compounds (**29–69**) to understand their structural requirements for the higher anticancer activity.

Biological activity and descriptors

As far as the 2D-QSAR analysis is concerned, the percentage tumor cell inhibition (%TCI) of these fortyone (41) synthesized compounds (**29–69**) was considered. These % TCI values were subsequently converted into the logarithmic scale [Log (%TCI)] and used as the dependent parameter. For a reliable and predictive 2D-QSAR modeling, selection of descriptors is the crucial criteria. As the biological activity and structural variations of these compounds **(29–69)** were comparatively less, keeping it in mind, atom-based descriptors as well as simple whole molecular descriptors were given importance for understanding the structural requirements for potential anticancer activity. The calculation of the atom-based quantum chemical descriptors was performed on (Chem 3D Pro version 5.0 and Chem Draw Ultra version 5.0 are programs of Cambridge Soft Corporation, USA) *Chem 3D Pro package* (CambridgeSoft

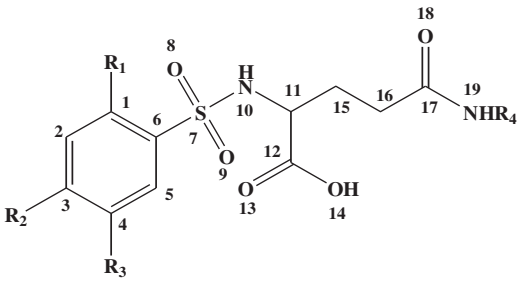

Fig. 3 Arbitrary numbering of 5-*N*-substituted-2-*N*-(substituted benzenesulphonyl)-L(+)glutamines **(29–69)**

Corporation, U.S.A.) and (Hyperchem Professional Release 7.0 is a computer program developed by Hypercube Inc., Gainesville, Florida) *Hyperchem Release 7.0 Pro Package* (Hypercube Inc., Gainesville, Florida). Molecules were numbered arbitrarily (shown in Fig. 3) keeping the serial number of atoms same in all molecules for atom-based descriptor calculations.

The energy minimization of these structures was done individually using molecular mechanical (MM+) force fields available in both of these softwares without cut-off for non-bonded interactions, solvation, and constrains. In *Chem 3D Pro. Package* software, further minimizations and charge calculations were performed under *MOPAC* module according to semi empirical Austin Model 1 (AM1) method (Leach 2001) using restricted Hartee-Fock (RHF): closed shell wave function whereas in *Hyperchem* software, these energy minimized structures were optimized geometrically by semi empirical AM1 method (Leach 2001) using the Polak-Ribiere algorithm with a RMS gradient of 0.1 kcal/Å mol. Wang-Ford charges of these atoms were calculated from the energy minimized geometry of these compounds by *Chem 3D Pro package* software. Frontier electron densities of these atoms were calculated by *Hyperchem Release 7.0 Pro Package* software. Simple whole molecular descriptors such as constitutional, atom-based fragments, geometrical, empirical descriptors were calculated by (DRAGON web version 2.1 is a QSAR software developed by Milano Chemometrics and QSAR Research Group, Dipartimento di Scienze dell'Ambiente e del Territorio Universitàdegli Studi di Milano—Bicocca) *Dragon* Software (Dragon 2.1 web version, Milano Bicocca). The Verloop STERIMOL parameters like L, B1 and B5 were collected from the literature (Krogsgaard–Larsen et al. 2002).

Division into training and test sets

Proper splitting of dataset into a test set and a training set is an essential criterion for unbiased predictive model development. In the current 2D-QSAR approach, two splitting methods, the *Y*-based ranking method (Hemmateenejad 2004) and *k*-means cluster analysis (Tropsha 2003; Snedecor and Cochran 1967) techniques were used for this purpose. In the *Y*-based ranking method, molecules were first ranked from the higher to the lower values of the observed biological activity. Then molecules in the 4th, 8th, 12th, and so on rows were collected and treated as the test set. The *k*-means cluster analysis separated and arranged different objects into groups according to their Euclidian distances in multidimensional space depending on the biological activity as well as those descriptors. From these clusters, the test set compounds were selected randomly.

Multiple regression analysis and variable selection

Multiple stepwise regression analysis was used for the selection of descriptors (Adhikari et al. 2015; Mondal et al. 2015; Mondal et al. 2014; Adhikari et al. 2014, 2013a, b; Mondal et al. 2013; Adhikari et al. 2012) by utilizing *F* value as the stepping criteria ($F = 3.0$ for inclusion, $F = 2.9$ for exclusion). Intercorrelated independent parameters (correlation coefficient > 0.50) were not considered and discarded during model development through stepwise regression analysis. Regression equations were evaluated by correlation coefficient (*R*), adjusted R^2 (R^2_a), variance ratio (*F*) at specified degrees of freedom (df), probability factor related to *F* ratio (*p*), standard error of estimate (SEE). Significant level of regression coefficient and intercepts of all equations were determined by using *t*-statistics and *p*-values of the corresponding parameters.

Validation of the QSAR models

As far as the validation of the developed model was concerned, leave-one-out (LOO) cross-validation method (Tetko et al. 2001) was used to validate models. Regarding the internal predictability parameters of the developed model, those were justified by predicted residual sum of squares (PRESS), cross-validated R^2 (R^2_{CV}), standard deviation error of prediction (SDEP) and standard error of PRESS (S_{PRESS}) whereas the external predictabilities of these models were judged by R^2_{Pred} values (Golbraikh and Tropsha 2002). The R^2_{CV} and the R^2_{Pred} value are calculated according to the following equations:

$$R^2_{CV} = 1 - \frac{\sum \left(Y_{Obs(Training)} - Y_{Pred(Training)}\right)^2}{\sum \left(Y_{Obs(Training)} - Y_{mean}\right)^2} \quad (1)$$

$$R^2_{Pred} = 1 - \frac{\sum \left(Y_{Obs(Test)} - Y_{Pred(Training)}\right)^2}{\sum \left(Y_{Obs(Test)} - Y_{mean}\right)^2} \quad (2)$$

In the Eq. (1), the Y_{mean} is the mean activity of the training set while the $Y_{Obs(training)}$ and the $Y_{pred(training)}$ are the experimental and predicted activity values of the

training set compounds respectively. A high R^2_{CV} value ($R^2_{CV} > 0.50$) indicates a good internal predictive ability of a model. In eq. (2) $Y_{Pred(Test)}$ and $Y_{Obs(Test)}$ are the predicted and the observed activity values of the test set compounds respectively and the Y_{mean} is the mean activity of the training set. The recommended value of R^2_{Pred} should be greater than 0.50 for successful predictability (Golbraikh and Tropsha 2002). The root mean square (r_m^2) value (Roy and Roy 2008) were also taken into consideration as an external predictability parameter. The recommended r_m^2 value should be more than 0.50. The r_m^2 is calculated as per the following equation:

$$r_m^2 = r^2 * \left[1 - \left(r^2 - r_0^2\right)^{1/2}\right] \quad (3)$$

In the Eq. (3), r^2 is the correlation coefficient between the observed and the predicted activity whereas r_0^2 is the correlation coefficient between the observed and the predicted activity passing through the origin. Applicability domain of a model is determined by the *extent of extrapolation* that considers the leverage values of compounds both in the test set and the training set in the developed model. Prediction is considered unreliable for compounds of leverage value greater than $3p/n$ where p is the number of model variables plus one and n is the number of the objects used to calculate the model (Tropsha et al. 2003). As stepwise regression procedure is susceptible to chance correlation, randomization test is performed where values of observed variance are scrambled randomly and repeatedly to generate the 2D-QSAR models. Resulting scores are compared with that of original 2D-QSAR models (generated from non-randomized activity values). If the original 2D-QSAR models are statistically significant, their regression coefficient (R) should be significantly greater than that of permuted data (Deswal and Roy 2006). In the current study, for 95% confidence interval, 19 trials were made (Nargotra et al. 2009) and average scrambled values were named as R^2_{SCR}. The best equation was selected by good internal predictability (justified by Q^2) and external predictability (justified by R^2_{Pred} and r_m^2) for the test set-training set combinations. An average Q^2 value of 0.60 and R^2_{Pred} and r_m^2 value of 0.50 were set as the selection criteria. The recommended ratio of the number of predictor parameters to number of data point of 1:5 was maintained in this work (Walker et al. 2003; Eriksson et al. 2003).

kNN-MFA 3D-QSAR study

The kNN-MFA is a popular 3D-QSAR technique and it was utilized for current 3D-QSAR molecular modeling study. The kNN-MFA 3D-QSAR analysis was done by using VLife QSAR Plus 1.0 (VLife Sciences and Technologies, India).

Alignment of molecules

The 3D structures of these compounds were drawn using the "draw molecule" function in VLife QSAR Plus 1.0 (VLife Science and Technologies, Pune, India). The MMFF94 force field and Gasteiger-Marsili charges followed by AM1 (Leach 2001) Hamiltonian method were used for the energy minimization of individual molecules as well as for the entire series with the convergence criterion of 0.001 kcal/mol Å. The location of each atom is vital for kNN-MFA study as the descriptor calculation is based on the 3D-space grid. Therefore, the mode to find out the conformation of each molecule and the method to align molecules together are two sensitive conditions to make a reasonable model. The lowest energy of the most active molecule of the dataset (compound **59**) was selected as the reference molecule to fit the training set and the test set compounds by using the align molecules function available with the software. The resulting aligned molecules were imported for building kNN-MFA 3D-QSAR models.

Dataset and sphere exclusion principle

Since a dataset of 41 compounds is a small dataset for kNN-MFA 3D-QSAR study, earlier reported 53 compounds (Samanta et al. 2004) are included in the dataset along with this 41 compounds to get a meaningful 3D-QSAR study. Selection of the training and the test set for kNN-MFA 3D-QSAR model was done by considering the fact that the test set compounds should express diversity in structures and a range of biological activities similar to the training set. The whole dataset was divided into the training set and the test set using sphere exclusion algorithm. This algorithm allows constructing the training sets covering all descriptor space areas occupied by representative points based on dissimilarity value. By setting dissimilarity value of 6.5, total 16 compounds were isolated from the dataset and treated as the test set. The remaining 78 compounds were used as the training set on which the model was developed.

Descriptor generation

To develop the kNN-MFA descriptor fields, a 3D cubic lattice with grid spacing of 2 Å in x, y, and z dimensions were formed to encompass these aligned molecules. The kNN-MFA descriptors were calculated to generate steric energies and electrostatic fields with default cut off energy of 10 and 30 kcal/mol respectively with an sp3 carbon probe atom having a Van der waals radius of 1.52 Å and a charge of +1.0. Gasteiger-Marsili charge was set for steric, electrostatic and hydrophobic energy calculations. The generated kNN-MFA steric and electrostatic fields were

scaled by the standard method in the software VLife QSAR Plus 1.0 (VLife Sciences and Technologies, Pune, India).

Evaluation of models

The statistical analysis of kNN field was done by the distance-based weighted average and the predictive value of the model was evaluated by standard LOO cross validation method (Tetko et al. 2001). The cross-validated correlation coefficient served as a measure of the quality of the model. The predictive r^2 calculation was based on molecules in the test set and was used to estimate validated r^2 by leave-one-out method (q^2), cross-validated standard error (q^2_se), predicted r^2 for external test set (pred_r^2) and standard error for predicted r^2 (pred_r^2se).

Molecular docking study

As these compounds are analogs of glutamine, it is assumed that this series of compounds may probably act through the competitive inhibition of glutaminase enzyme. Based on the assumption, the best active compound (compound **59**) was docked against the human kidney type glutaminase enzyme (KGA). Molecular docking study was performed in GOLD molecular docking tools (Astex Technology, Chembridge, UK, 2011; Jones et al. 1995).

Protein structure

The X-ray crystallographic structure of human phosphate dependent kidney type glutaminase (KGA) was docked with the best active compound (compound **59**). The PDB structure of human glutaminase in complex with L-glutamic acid (PDB ID 3CZD) was downloaded from the Research Collaborator for Structural Bioinformatics web site (www.rscb.org). The X-ray crystal structure had the resolution of 2.40 Å. Glutaminase forms a homodimer and each monomer is bifurcated fold with the active site between the two domains. The first domain is comprised of five stranded anti-parallel β-sheet surrounded by α-helices and loops (residues 222–281 and 424–531). The second domain is completely α-helical (residues 282–423). In the inter-domain cleft, L-glutamic acid was added to the protein during crystallization. It made hydrogen bonds with Gln285, Ser286, Asn335, Glu381, Asn388, Tyr414, Tyr466, and Val484. The inhibition of human kidney type glutaminase (KGA) by glutamic acid was reported earlier (www.rscb.org.; www.thesgc.org/structures/structure_description/3CZD/).

It was also reported (www.thesgc.org/structures/structure_description/3CZ) that although Lys289 and Ser286 are present in close proximity, Ser286 makes hydrogen bonding with the carboxyl group of the bound glutamic acid. Glutamic acid forms hydrophobic interactions with Val484, Ser 286, and Tyr249.

Docking procedure

GOLD v5.0.1 (Astex Technology, Chembridge, UK, 2011) was used to predict the binding of flexible molecules to the protein binding site. Generic algorithm incorporated into GOLD v5.0.1 software was used for the ligand-protein docking that allows full ligand and partial protein flexibility (Jones et al. 1997). As far as the docking is concerned, the ligand binding site was defined as a 8 Å radius from bound ligand and used as an input for GOLD calculations. Default GOLD fitness functions and default evolutionary parameters such as population size = 100; selection pressure = 1.1, operations = 1,00,000, island = 2, niche size = 2, migration = 10, mutation = 95, crossover = 95 were used during docking calculations. Ten docking runs were performed per structure unless three of the 10 poses were within 1.5 Å RMSD of each other. For understanding the interaction ability of these compounds, Goldscore was considered. The more the GOLD fitness score, the better is the binding ability of the ligand.

MD simulation

As far as the MD simulation was concerned, based on the docking interactions, it was performed on the apo, glutamic acid bound and compound-59 bound complexes of glutaminase (KGA). The GROMACS 4.0.4 program (Hess et al. 2008; Van Der Spoel et al. 2005) with GROMOS96 43al force field at constant temperature and pressure ensemble was used for performing all these simulation analyses. In the MD simulations, all these protein atoms were surrounded by a cubic water box pf SPC3 water molecules that extended 10 Å away from the protein and periodic boundary conditions were applied in all directions. These systems were neutralized with Na^+ and Cl^- counter ions replacing the solvent molecules. Energy minimization was performed using the steepest descent algorithm for 10000 steps. A 100 ps position restrained MD simulation was performed for every system followed by 500 ps production of MD simulations with a time step of 2 fs a constant pressure (1 atm) and temperature (300 K). The electrostatic interaction was calculated by the Particle-Mesh Ewald (PME) method. All bonds were constrained using LINCS algorithm. The GROMACS topology for the ligands was obtained from PRODRG web server. The stability of the protein complexes in the MD simulation was also monitored using the root mean square deviation (RMSD) calculation with respect to their initial structure. The RMSD of glutaminase-glutamic acid substrate complex showed the lowest value

compared to all other systems. The complex of glutaminase and the best active compound (compound **59**) showed considerably lower RMSD value which indicates the stability of this complex. All complexes in these simulations except the apoform of the enzyme converged at around 2.0 Å.

Results and discussion

Chemistry

Substituted benzenesulphonyl chlorides **(8–14)** were prepared from the corresponding substituted benzenes **(1–7)** through chlorosulphonylation (Huntress and Carten 1940). To obtain 2-N-(substituted benzenesulphonyl)–L(+) glutamic acids **(15–21)**, these sulphonyl chlorides **(8–14)** were condensed separately with L(+) glutamic acid. During the condensation process, alkaline medium (2 N NaOH) was maintained that helped to remove hydrochloric acid formed. The resulting diacids **(15–21)** were subjected to cyclization reaction with acetyl chloride to get 1-*N*-(substituted benzenesulphonyl)-5-oxopyrrolidine-2-carboxylic acids **(21–28)**. Aminolysis of these monoacids **(21–28)** separately with various amines produced the corresponding glutamine analogs **(29–69)** (Fig. 1).

The route of synthesis of these glutamines **(29–69)** was presented schematically in Fig. 2. The structures and physical data of the intermediate compounds are shown in Table 1.

The structures and physical data of the final compounds (**29–69**) are shown in Table 2.

All title compounds (**29–69**) were obtained as crystalline solids with appreciable yields except two (compounds **35** and **36**). Spectral and elemental analysis data of all the final compounds (**29–69**) are shown below:

*Compound **29***

Yield 44.74%, M. P. 174–176 °C, MS (FAB):M+H^+ peak at *m/z* 407. IR (KBr, cm^{-1}): 3103 (N–H str. of CONH), 2925 (ali C–H str.), 1755(C=O str.), 1697, 1450 (ali C–H def.), 1481, 1367 (NO_2 str.), 1340(S=O str. of SO_2NH, asymmetric), 1176 (S=O str. of SO_2NH, symmetric), 1087, 1024, 958, 756 (Ar–C–H def.). ^1H NMR (300 MHz, CDCl3): δ 12.65 (s, 1H, COOH), δ 8.23-7.9 (m, 4H, nitrobenzyl protons), 7.87 (dd, J = 13.3, 2H, H-2′, H-6′), 7.72 (d, 1H, H-4′), δ 7.42(dd, 2H, J = 5.7, H-3′, H-5′), δ 3.78 (m, 1H, H-2), δ 2.19 (m, 2H, H-4), δ 2.11–1.99 (m, 2H, HA-3, HB-3). Anal. (C, H, N) calcd: 50.12, 4.17, 10.32; found: 50.31, 4.67, 10.39

Table 1 Physical data of the intermediate compounds (**8–28**)

Cpd[a]	R1	R2	R3	Mp(°C)	% Yield	Molecular formula
8	H	H	H	Liquid	[b]	$C_6H_5SO_2Cl$
9	H	OCH_3	H	40–42	71.32	$C_7H_7SO_3Cl$
10	OCH_3	H	OCH_3	105–108	91.56	$C_8H_9SO_4Cl$
11	CH_3	CH_3	H	Liquid	79.57	$C_8H_9SO_2Cl$
12	H	*i*-C_4H_9	H	Liquid	81.26	$C_{10}H_{13}SO_2Cl$
13	H	F	H	Liquid	80.44	$C_6H_4SO_2ClF$
14	CH_3	H	CH_3	Liquid	97.56	$C_8H_9SO_2Cl$
15	H	H	H	125–127	84.56	$C_{11}H_{13}O_6NS$
16	H	OCH_3	H	75–78	37.75	$C_{12}H_{15}O_7NS$
17	OCH_3	H	OCH_3	87–89	50.52	$C_{13}H_{17}O_8NS$
18	CH_3	CH_3	H	135–141	49.92	$C_{13}H_{17}O_6NS$
19	H	*i*-C_4H_9	H	132–134	85.53	$C_{15}H_{21}O_6NS$
20	H	F	H	125–127	78.93	$C_{11}H_{12}O_6NSF$
21	CH_3	H	CH_3	102–104	82.46	$C_{13}H_{17}O_6NS$
22	H	H	H	145–147	56.66	$C_{11}H_{11}NO_5S$
23	H	OCH_3	H	95–97	81.53	$C_{12}H_{13}NO_6S$
24	OCH_3	H	OCH_3	124–126	82.26	$C_{13}H_{15}$ NO_7S
25	CH_3	CH_3	H	173–175	85.55	$C_{13}H_{15}$ NO_5S
26	H	*i*-C_4H_9	H	112–114	86.12	$C_{15}H_{19}NO_5S$
27	H	F	H	78–80	72.13	$C_{11}H_{10}FNO_5S$
28	CH_3	H	CH_3	82–84	90.25	$C_{13}H_{15}NO_5S$

[a] Compound number;

[b] Directly purchased from Spectrochem, Mumbai

*Compound **30***

Yield 81.48%, M. P. 178–180 °C, MS (FAB):M+H^+ peak at *m/z* 372. IR (KBr, cm^{-1}): 3467, 3110 (N–H str. of CONH), 2977 (Ar C–H str.), 2839 (ali C–H str.), 1701 (C=O str.), 1552, 1444 (ali C–H def.), 1307 (S=O str. of SO_2NH,asymmetric), 1255 (asymmetric C–O–C str), 1151 (S=O str. of SO_2NH, symmetric), 1099 (symmetric C–O–C str),991,829,804 (Ar–C–H def.). ^1H NMR (300 MHz, CDCl3): δ 12.51 (s, 1H, COOH), δ 7.69 (d, 1H, H-3′, H-5′), δ 7.67 (m, 1H, CONH-5), δ 7.58 (s, 1H, SO_2NH), δ 7.47 (d, 2H, H-2′, H-6′), δ 3.93 (m, 1H, H-2), 1.47-1.26 (m, 9H, three CH_3 of t-But), 2.23 (m, 2H, H-4), 2.07–1.92 (m, 2H, HA-3, HB-3). Anal. (C, H, N) calcd: 51.61, 6.45, 7.53; found: 51.75, 6.58, 7.42

*Compound **31***

Yield 86.09%, M. P. 90-92 °C, MS (FAB):M+H^+ peak at *m/z* 437. IR (KBr, cm^{-1}): 3533, 3110 (N–H str. of CONH), 2975 (Ar C–H str.), 2839 (ali C–H str.), 1733 (C=O str.), 1531, 1461 (ali C–H def.), 1350 (S=O str. of SO_2NH, asymmetric), 1269 (asymmetric C-O-C str), 1161 (S=O str.

Table 2 Structures and the physicochemical data of 5-*N*-substituted-2-*N*-(substituted benzenesulphonyl)-L(+) glutamines **(29–69)**

Cpd[a]	R_1	R_2	R_3	R_4	Mp(°C)	% Yield	%TCI[e]	Log(%TCI)[f]
29	H	H	H	$C_6H_4NO_2$	174–176	44.74	5.00	0.699
30	H	OCH_3	H	*t*-C_4H_9	178–180	81.48	57.57	1.760
31	H	OCH_3	H	$C_6H_4NO_2$	90–92	86.09	46.81	1.670
32	H	OCH_3	H	$C_2H_4C_6H_5$	131–133	89.13	21.58	1.334
33	OCH_3	H	OCH_3	H	145–147	57.14	39.83	1.600
34	OCH_3	H	OCH_3	CH_3	122–124	44.75	47.48	1.676
35	OCH_3	H	OCH_3	C_2H_5	73–75	16.11	53.60	1.729
36	OCH_3	H	OCH_3	*n*-C_3H_7	65–67	14.83	67.23	1.827
37	OCH_3	H	OCH_3	*n*-C_4H_9	111–113	53.80	66.96	1.826
38	OCH_3	H	OCH_3	*t*-C_4H_9	171–173	87.42	74.11	1.870
39	OCH_3	H	OCH_3	*n*-C_6H_{13}	52–54	67.21	51.84	1.715
40	OCH_3	H	OCH_3	*c*-C_6H_{11}	148–150	56.68	61.13	1.786
41	OCH_3	H	OCH_3	$CH_2C_6H_5$	162–164	73.46	51.41	1.711
42	OCH_3	H	OCH_3	$C_2H_4C_6H_5$	160–162	92.67	31.30	1.495
43	CH_3	CH_3	H	H	150–152	75.63	85.26	1.931
44	CH_3	CH_3	H	CH_3	137–139	47.26	53.90	1.840
45	CH_3	CH_3	H	C_2H_5	130132	62.13	80.38	1.905
46	CH_3	CH_3	H	*n*-C_3H_7	137–139	54.26	38.82	1.589
47	CH_3	CH_3	H	*i*-C_3H_7	148–150	64.14	61.64	1.790
48	CH_3	CH_3	H	*i*-C_4H_9	150–152	89.64	62.37	1.795
49	CH_3	CH_3	H	*n*-C_5H_{11}	143–145	78.35	63.56	1.803
50	CH_3	CH_3	H	*n*-C_6H_{13}	152–154	69.53	56.85	1.755
51	CH_3	CH_3	H	C_6H_5	200–203	84.81	79.26	1.899
52	CH_3	CH_3	H	$C_6H_4NO_2$	173–175	72.40	56.60	1.753
53	CH_3	CH_3	H	$C_2H_4C_6H_5$	147–149	86.65	56.51	1.752
54	H	*i*-C_4H_9	H	H	141–143	89.05	75.76	1.879
55	H	*i*-C_4H_9	H	CH_3	173–175	96.99	28.19	1.450
56	H	*i*-C_4H_9	H	*i*-C_3H_7	155–157	76.27	65.04	1.813
57	H	*i*-C_4H_9	H	*n*-C_4H_9	173–175	77.55	79.58	1.847
58	H	*i*-C_4H_9	H	*i*-C_4H_9	173–175	77.55	88.38	1.946
59	H	*i*-C_4H_9	H	*n*-C_5H_{11}	165–167	78.74	90.92	1.959
60	H	*i*-C_4H_9	H	*c*-C_6H_{11}	179–181	74.69	28.50	1.455
61	H	*i*-C_4H_9	H	C_6H_5	202–204	91.12	62.87	1.798
62	H	*i*-C_4H_9	H	$CH_2C_6H_5$	102–104	98.18	63.17	1.800
63	H	F	H	CH_3	133–135	48.34	67.46	1.829
64	H	F	H	*t*-C_4H_9	193–195	52.86	37.96	1.579
65	H	F	H	$C_6H_4NO_2$	166–168	79.52	16.46	1.216
66	H	F	H	$C_2H_4C_6H_5$	119–121	83.59	68.20	1.834
67	CH_3	H	CH_3	t-C_4H_9	171–173	94.61	79.75	1.902
68	CH_3	H	CH_3	$C_6H_4NO_2$	99–101	48.36	63.26	1.801
69	CH_3	H	CH_3	$C_2H_4C_6H_5$	130–132	89.43	39.46	1.596
Mito[b]	–	–	–	–	–	–	100.00	–
Aza[c]	–	–	–	–	–	–	100.00	–
DN[d]	–	–	–	–	–	–	100.00	–

[a] Compound number;

[b] Mitomycin,

[c] Azaserine;

[d] DON;

[e] %Tumor cell inhibition;

[f] Logarithm of tumor cell inhibition

of SO_2NH, symmetric), 1089 (symmetric C-O-C str), 960, 842, 742 (Ar–C–H def.). ^{1}H NMR (300 MHz, CDCl3): δ 12.56 (s, 1H, COOH), δ 7.83-7.66 (m, 5H, phenyl protons), *δ* 7.11 (dd, 2H, J = 7.2, H-3′, H-5′), *δ* 7.08 (d, 2H, H-2′, H-6′), *δ* 7.45 (s, 1H, SO_2NH), *δ* 3.87 (s, 3H, OCH_3), *δ* 3.78 (m, 1H, H-2), *δ* 2.30 (m, 2H, H-4), *δ* 1.99–1.92 (m, 2H, HA-3, HB-3). Anal. (C, H, N) calcd: 49.43, 4.35, 9.61; found: 49.76, 4.16, 9.84

Compound ***32***

Yield 89.13%, M. P. 131–133 °C, MS (FAB):M+H^+ peak at *m/z* 420. IR (KBr, cm^{-1}): 3396, 3259 (N–H str. of CONH), 3028 (ArC–H str.), 2837 (ali C–H str.), 1712(C=O str.), 1542, 1454 (ali C–H def.), 1301 (S=O str. of SO_2NH, asymmetric), 1257 (asymmetric C–O–C str), 1159 (S=O str. of SO_2NH, symmetric), 1091 (symmetric C–O–C str), 975, 831, 746 (Ar–C–H def.). ^1H NMR (300 MHz, CDCl3): δ 12.58 (s, 1H, COOH), 7.11 (d, 2H, H-3′, H-5′), 7.08 (dd, J = 12.8, 2H, H-2′, H-6′), *δ* 7.45 (s, 1H, SO_2NH), *δ* 3.87 (s, 3H, OCH_3), *δ* 3.69 (m, 1H, H-2), 2.30 (m, 2H, H-4), *δ* 1.99–1.92 (m, 2H, HA-3, HB-3). Anal. (C, H, N) calcd: 57.14, 5.71, 6.67; found: 57.43, 5.68, 6.73

Compound ***33***

MS (FAB):M+H^+ peak at *m/z* 334. IR (KBr, cm^{-1}): 3465, 3334 (N–H str. of $CONH_2$), 3083 (ArC–H str.), 2840 (ali C–H str.), 1716 (C=O str.), 1579, 1456 (ali C–H def.), 1307 (S=O str. of SO_2NH, asymmetric), 1278 (asymmetric C–O–C str), 1164 (S=O str. of SO_2NH, symmetric), 1043 (symmetric C–O–C str), 945, 790, 740 (Ar–C–H def.). ^1H NMR (300 MHz, CDCl3): *δ* 12.62 (s, 1H, COOH), *δ* 7.64 (d, 1H, J = 6.8, H-3′), *δ* 7.27 (d, 1H, H-4′), *δ* 7.05 (s, 1H, H-6′), *δ* 6.75 (m, 2H, $CONH_2$), *δ* 3.82 (s, 3H, 5′ OCH_3), *δ* 3.74 (s, 3H, 2′ OCH_3), *δ* 3.68 (m, 1H, H-2), *δ* 2.14 (m, 2H, H-4), *δ* 1.85-1.65(m, 2H, H-3). Anal. (C, H, N) calcd: 43.11, 5.39, 8.38; found: 43.24, 5.41, 8.54

Compound ***34***

MS (FAB):M+H^+ peak at *m/z* 360. IR (KBr, cm^{-1}): 3296, 3112 (N–H str. of CONH), 3002 (ArC–H str.), 2925, 2840 (ali C–H str.), 1714 (C=O str.), 1531, 1438 (ali C–H def.), 1307 (S=O str. of SO_2NH, asymmetric), 1240 (asymmetric C–O–C str), 1166 (S=O str. of SO_2NH, symmetric), 1047 (symmetric C–O–C str),977, 823, 790 (Ar–C–H def.). ^1H NMR (300 MHz, CDCl3): *δ* 12.61 (s, 1H, COOH), *δ* 7.62 (d, J = 4.6, 1H, H-3′), *δ* 7.31 (d, J = 2.4, 1H, H-4′), *δ* 7.05 (s, 1H, H-6′), *δ* 6.78 (m, 2H, $CONH_2$), *δ* 3.87 (s, 3H, 5′ OCH_3), *δ* 3.76 (s, 3H, 2′ OCH_3), *δ* 3.68 (m, 1H, H-2), *δ* 2.60 (m, 3H, N-CH_3-1″), δ 2.16 (m, 2H, H-4), *δ* 1.85-1.65(m, 2H, H-3). Anal. (C, H, N) calcd: 46.67, 5.55, 7.78; found: 46.84, 5.46, 7.78

Compound ***35***

MS (FAB):M+H^+ peak at *m/z* 374. IR (KBr, cm^{-1}): 3361, 3124 (N–H str. of CONH), 2974 (Ar C–H str.), 2925 (ali C–H str.), 1706 (C=O str.), 1550, 1442 (ali C–H def.), 1309 (S=O str. of SO_2NH, asymmetric), 1228 (asymmetric C–O–C str), 1161 (S=O str. of SO_2NH, symmetric), 1041 (symmetric C-O-C str),983, 827(Ar–C–H def.). ^1H NMR (300 MHz, CDCl3): *δ* 12.67 (s, 1H, COOH), 7.62 (d, J = 4.3, 1H, H-3′), 7.31 (d, J = 1.8, 1H, H-4′), 7.05 (s, 1H, H-6′), 6.78 (m, 2H, $CONH_2$), 3.87 (s, 3H, 5′ OCH_3), 3.80 (m, 2H, N-CH_2-1″),3.76 (s, 3H, 2′ OCH_3), 3.68 (m, 1H, H-2), *δ* 2.60 (m, 3H, N-CH_3-1‴), 2.16 (m, 2H, H-4), *δ* 1.22 (m, 3H, CH_3-2″). Anal. (C, H, N) calcd: 48.13, 5.88, 7.49; found: 48.24, 5.81, 7.54

Compound ***36***

MS (FAB):M+H^+ peak at *m/z* 388. IR (KBr, cm^{-1}): 3357, 3286 (N–H str. of CONH), 3097 (Ar C–H str.), 2937 (ali C–H str.), 1706 (C=O str.), 1554, 1440(ali C–H def.), 1299 (S=O str. of SO_2NH, asymmetric), 1226 (asymmetric C–O–C str), 1159 (S=O str. of SO_2NH, symmetric), 1039 (symmetric C–O–C str),983, 825,746 (Ar–C–H def.). ^1H NMR (300 MHz, CDCl3): *δ* 12.56 (s, 1H, COOH), *δ* 7.62 (d, J = 3.5, 1H, H-3′), *δ* 7.34 (d, J = 1.9, 1H, H-4′), *δ* 6.80 (m, 2H, $CONH_2$), *δ* 3.88 (s, 3H, 5′ OCH_3), *δ* 3.74 (s, 3H, 2′ OCH_3), *δ* 3.63 (m, 1H, H-2), *δ* 3.34 (m, 2H, N-CH_2-1″), δ 2.66 (m, 3H, N-CH_3-1‴), δ 2.16 (m, 2H, H-4), *δ* 1.22 (m, 3H, CH_3-2″), δ 1.65 (m, 2H, CH_2-2‴), *δ* 0.97 (m, 3H, CH_3-3‴). Anal. (C, H, N) calcd: 49.48, 6.18, 7.22; found: 49.64, 6.17, 7.24

Compound ***37***

MS (FAB):M+H^+ peak at *m/z* 402. IR (KBr, cm^{-1}): 3299 (N–H str. of CONH),3083 (Ar C–H str.), 2958 (ali C–H str.), 1720 (C=O str.), 1546, 1442 (ali C–H def.), 1328 (S=O str. Of SO_2NH, asymmetric), 1247 (asymmetric C–O–C str), 1157 (S=O str. of SO_2NH, symmetric), 1045(symmetric C–O–C str), 989, 806, 740 (Ar–C–H def.). ^1H NMR (300 MHz, CDCl3): δ 12.52 (s, 1H, COOH), 7.62 (d,J = 5.6, 1H, H-3′), 7.31 (d, J = 2.1, 1H, H-4′), 7.05 (s, 1H, H-6′), 6.78 (m, 2H, $CONH_2$), 3.87 (s, 3H, 5′ OCH_3), 3.76 (s, 3H, 2′ OCH_3), 3.68 (m, 1H, H-2), *δ* 3.29 (m, 2H, N-CH_2-1″), 2.16 (m, 2H, H-4), *δ* 1.22 (m, 3H, CH_3-2″), 1.49-1.33 (m, 4H, CH_2-2″, CH_2-3″), 0.99–0.93 (m, 3H, CH_3-4″). Anal. (C, H, N) calcd: 50.75, 6.47, 6.96; found: 50.87, 6.51, 7.06

Compound ***38***

MS (FAB):M+H^+ peak at m/z 402. IR (KBr, cm^{-1}): 3203, 3101 (N–H str. of CONH), 2977 (Ar C–H str.), 2918 (ali C–H str.), 1701 (C=O str.), 1537, 1498 (ali C–H def.), 1319 (S=O str. of SO_2NH, asymmetric), 1224 (asymmetric C-O-C str), 1155 (S=O str. of SO_2NH, symmetric), 1037 (symmetric C-O-C str), 990, 829, 804 (Ar–C–H def.). ^1H NMR (300 MHz, CDCl3): *δ* 12.52 (s, 1H, COOH), 7.52-7.10 (m, 4H, Phenyl protons), 6.78 (m, 2H, $CONH_2$), 3.87 (s, 3H, 5′ OCH_3), 3.76 (s, 3H, 2′ OCH_3), 3.68 (m, 1H, H-2),

2.16 (m, 2H, H-4), 1.46-1.27 (m, 9H, three methyl groups of t-But). Anal. (C, H, N) calcd: 50.75, 6.47, 6.96; found: 50.87, 6.45, 7.12

Compound ***39***

MS (FAB):M+H^+ peak at *m/z* 430. IR (KBr, cm^{-1}): 3305, (N–H str. of CONH), 3082 (Ar C–H str.), 2931 (ali C–H str.), 1649 (C=O str.), 1550, 1442 (ali C–H def.), 1326 (S=O str. of SO_2NH, asymmetric), 1224 (asymmetric C–O–C str), 1159 (S=O str. of SO_2NH, symmetric), 1045 (symmetric C–O–C str),929, 806, 700 (Ar–C–H def.). ^1H NMR (300 MHz, CDCl3): δ 12.52 (s, 1H, COOH), 7.52–7.10 (m, 4H, Phenyl protons), 6.78 (m, 2H, $CONH_2$), 3.87 (s, 3H, 5′ OCH_3), 3.76 (s, 3H, 2′ OCH_3), 3.68 (m, 1H, H-2), δ 3.21 (m, 2H, NH-CH_2-1″), 2.16 (m, 2H, H-4), δ 1.22 (m, 3H, CH_3-2″), δ 0.83–1.63 (m, 13H, CH_2-2″, CH_2-3″, CH_2-4″, CH_2-5″, CH_2-6″,). Anal. (C, H, N) calcd: 53.02, 6.98, 6.51; found: 53.17, 6.99, 7.65

Compound ***40***

MS (FAB):M+H^+ peak at *m/z* 428. IR (KBr, cm^{-1}): 3379, 3286 (N–H str. of CONH), 2991 (Ar C–H str.), 2935 (ali C–H str.), 1733 (C=O str.), 1553, 1463 (ali C–Hdef.), 1332 (S=O str. of SO_2NH, asymmetric), 1222 (asymmetric C-O-C str), 1159 (S=O str. of SO_2NH, symmetric), 1049 (symmetric C–O–C str),977, 796, 744 (Ar–C–H def.). ^1H NMR (300 MHz, CDCl3): δ 12.62 (s, 1H, COOH), 7.64 (d, J = 5.8, 1H, H-3′), 7.27 (d, J = 1.6, 1H, H-4′), 7.05 (s, 1H, H-6′), 6.75 (m, 2H, $CONH_2$), 3.82 (s, 3H, 5′ OCH_3), 3.74 (s, 3H, 2′ OCH_3), 3.68 (m, 1H, H-2), 2.14 (m, 2H, H-4), 1.85–1.65(m, 2H, H-3), δ 1.01-1.90 (m, 22H, Cyclohexyl protons). Anal. (C, H, N) calcd: 53.27, 6.54, 6.54; found: 53.45, 6.52, 6.69

Compound ***41***

MS (FAB):M+H^+ peak at *m/z* 436. IR (KBr, cm^{-1}): 3316, 3106 (N–H str. of CONH), 3012 (Ar C–H str.), 2876 (ali C–H str.), 1700 (C=O str.), 1556, 1440 (ali C–H def.), 1332 (S=O str. of SO_2NH, asymmetric), 1247 (asymmetric C–O–C str), 1160 (S=O str. of SO_2NH, symmetric), 1045 (symmetric C–O–C str), 977, 798, 748 (Ar–C–H def.). ^1H NMR (300 MHz, CDCl3): δ 12.63 (s, 1H, COOH), 7.66 (d, J = 5.8, 1H, H-3′), 7.25 (d, 1H, J = 2.4, H-4′), 7.03 (s, 1H, H-6′), 6.72 (m, 2H, $CONH_2$), 3.80 (s, 3H, 5′ OCH_3), 3.72 (s, 3H, 2′ OCH_3), 3.60 (s, 2H, N-CH_2-1″), 2.18 (m, 2H, H-4), 1.86-1.65(m, 2H, H-3). Anal. (C, H, N) calcd: 55.04, 5.50, 6.42; found: 55.16, 5.56, 6.56

Compound ***42***

MS (FAB):M+H^+ peak at *m/z* 450. IR (KBr, cm^{-1}): 3303 (N–H str. of CONH), 3026 (Ar C–H str.), 2939 (ali C–H str.), 1542, 1440 (ali C–H def.), 1336 (S=O str. of SO_2NH, asymmetric), 1234 (asymmetric C–O–C str), 1153 (S=O str. of SO_2NH, symmetric), 1033 (symmetric C–O–C str), 817, 746 (Ar–C–H def.). ^1H NMR (300 MHz, CDCl3): δ 12.64 (s, 1H, COOH), 7.64 (d, J = 6.2, 1H, H-3′), 7.27 (d, 1H, H-4′), 7.05 (s, 1H, H-6′), 6.75 (m, 2H, $CONH_2$), 3.82 (s, 3H, 5′ OCH_3), 3.74 (s, 3H, 2′ OCH_3), 3.69 (s, 2H, N-CH_2-1″), 2.77 (m, 2H, CH_2-2″) 2.14 (m, 2H, H-4), 1.85-1.65 (m, 2H, H-3). Anal. (C, H, N) calcd: 56.00, 5.78, 6.22; found: 56.15, 5.87, 6.45

Compound ***43***

MS (FAB):M+H^+ peak at *m/z* 302. IR (KBr, cm^{-1}): 3346, (N–H str. of CONH), 3056 (Ar C–H str.), 2860 (ali C–H str.), 1716 (C=O str.), 1595, 1448 (ali C–H def.), 1344 (S=O str. of SO_2NH, asymmetric), 1149 (S=O str. of SO_2NH, symmetric), 973, 781, 705 (Ar–C–H def.). ^1H NMR (300 MHz, CDCl3): δ 12.56 (s, 1H, COOH), 7.28 (d, J = 7.2, 1H, H-3′), 7.20 (d, J = 2.3, 1H, H-4′), 7.48 (s, 1H, SO_2NH), 6.75 (m, 2H, $CONH_2$), 3.66 (m, 1H, H-2), 2.27 (m, 2H, H-4), 2.02-2.07 (m, 2H, H-3),1.70- 0.99 (m, 6H, six methyl protons of xylene). Anal. (C, H, N) calcd: 47.68, 5.96, 9.27; found: 47.77, 5.99, 9.23

Compound ***44***

MS (FAB):M+H^+ peak at *m/z* 328. IR (KBr, cm^{-1}): 3339, 3253 (N–H str. of CONH), 3062 (Ar C–H str.), 2931 (ali C–H str.), 1714 (C=O str.), 1537, 1494 (ali C–H def.), 1323 (S=O str. of SO_2NH, asymmetric), 1155 (S=O str. of SO_2NH, symmetric), 972,771, 713 (Ar–C–H def.). ^1H NMR (300 MHz, CDCl3): δ 12.63 (s, 1H, COOH), 7.28 (d, J = 6.5, 1H, H-3′), 7.24 (d, J = 1.4, 1H, H-4′), 7.48 (s, 1H, SO_2NH), 6.72 (m, 2H, $CONH_2$), 3.64 (m, 1H, H-2), δ 2.67 (m, 3H, N-CH_3-1‴), 2.24 (m, 2H, H-4), 2.02-2.06 (m, 2H, H-3),1.63- 0.97 (m, 6H, six methyl protons of xylene). Anal. (C, H, N) calcd: 51.22, 6.10, 8.54; found: 51.43, 5.97, 8.45

Compound ***45***

MS (FAB):M+H^+ peak at *m/z* 342. IR (KBr, cm^{-1}): 3373, 3251 (N–H str. of CONH), 2974 (Ar C–H str.), 2931 (ali C–H str.), 1718 (C=O str.), 1564, 1452 (ali C–H def.), 1323 (S=O str. of SO_2NH, asymmetric), 1157 (S=O str. of SO_2NH, symmetric), 975, 798, 750 (Ar–C–H def.). ^1H NMR (300 MHz, CDCl3): δ 12.63 (s, 1H, COOH), δ 7.28 (d, 1H, H-3′), δ 7.24 (d, 1H, H-4′), δ 7.48 (s, 1H,

SO_2NH), δ 7.23 (m, 1H, CONH), δ 3.64 (m, 1H, H-2), δ 2.67 (m, 3H, N-CH_3-1‴), 2.24 (m, 2H, H-4), 2.02-2.06 (m, 2H, H-3),1.63–0.97 (m, 6H, six methyl protons of xylene). Anal. (C, H, N) calcd: 52.63, 6.43, 8.19; found: 52.95, 6.55, 8.32

Compound ***46***

MS (FAB):M+H^+ peak at *m/z* 356. IR (KBr, cm^{-1}): 3377, 3251 (N–H str. of CONH), 3060 (Ar C–H str.), 2875 (ali C–H str.), 1716 (C=O str.), 1564, 1454 (ali C–H def.), 1323 (S=O str. of SO_2NH, asymmetric), 1155 (S=O str. of SO_2NH, symmetric), 972, 773, 709 (Ar–C–H def.). ^{1}H NMR (300 MHz, CDCl3): δ 12.66 (s, 1H, COOH), δ 7.28 (d, 1H, H-3′), δ 7.24 (d, J = 1.9, 1H, H-4′), δ 7.48 (s, 1H, SO_2NH), δ 7.23 (m, 1H, CONH), δ 3.64 (m, 1H, H-2), δ 2.67 (m, 3H, N-CH_3-1‴), 2.24 (m, 2H, H-4), δ 2.02–2.06 (m, 2H, H-3),δ 1.63–0.97 (m, 6H, six methyl protons of xylene), δ 1.22 (m, 3H, CH_3-2″). Anal. (C, H, N) calcd: 53.93, 6.74, 7.86; found: 54.13, 6.77, 7.94

Compound ***47***

MS (FAB):M+H^+ peak at *m/z* 356. IR (KBr, cm^{-1}): 3377, 3272 (N–H str. of CONH), 2972 (Ar C–H str.), 2875 (ali C–H str.), 1718 (C=O str.), 1558, 1450 (ali C–H def.), 1340 (S=O str. of SO_2NH, asymmetric), 1157 (S=O str. of SO_2NH, symmetric), 983, 831, 703 (Ar–C–H def.). ^{1}H NMR (300 MHz, CDCl3): δ 12. 45 (s, 1H, COOH), 7.30 (s, 1H, H-3′), 7.21 (s, 1H, H-4′), 7.43 (s, 1H, SO_2NH), δ 3.55 (m, 1H, N-CH-1,‴), 2.27 (m, 2H, H-4), 2.02-2.07 (m, 2H, H-3), 1.63–0.97 (m, 6H, six methyl protons of xylene), δ 1.22-1.18 (m, 6H, CH_3-2″, CH_3-3‴). Anal. (C, H, N) calcd: 53.93, 6.74, 7.86; found: 54.11, 6.76, 7.55

Compound ***48***

MS (FAB):M+H^+ peak at *m/z* 370. IR (KBr, cm^{-1}): 3377, 3271 (N–H str. of CONH), 2952 (Ar C–H str.), 2866 (ali C–H str.), 1718 (C=O str.), 1571, 1450 (ali C–H def.), 1323 (S=O str. of SO_2NH, asymmetric), 1157 (S=O str. of SO_2NH, symmetric), 983, 767, 727 (Ar–C–H def.). ^{1}H NMR (300 MHz, CDCl3): δ 12.54 (s, 1H, COOH), 7.34 (s, 1H, H-3′), 7.23 (s, 1H, H-4′), 7.41 (s, 1H, SO_2NH), δ 2.67 (m, 2H, N-CH_2-1‴), 2.28 (m, 2H, H-4), 2.00–2.07 (m, 2H, H-3), 1.65–0.98 (m, 6H, six methyl protons of xylene), 0.92–0.84 (m, 7H, CH-2″, CH_3-3″, CH_3-4″). Anal. (C, H, N) calcd: 55.13, 7.03, 7.57; found: 55.42, 7.02, 7.85

Compound ***49***

MS (FAB):M+H^+ peak at *m/z* 384. IR (KBr, cm^{-1}): 3377, 3253 (N–H str. of CONH), 3060 (Ar C–H str.), 2867 (ali C–H str.), 1716 (C=O str.), 1564, 1454 (ali C–H def.), 1323 (S=O str. of SO_2NH, asymmetric), 1155 (S=O str. of SO_2NH, symmetric), 973, 771, 711 (Ar–C–H def.). ^{1}H NMR (300 MHz, CDCl3): δ 12.57 (s, 1H, COOH), 7.34 (s, 1H, H-3′), 7.23 (s, 1H, H-4′), 7.41 (s, 1H, SO_2NH), δ 2.67 (m, 2H, N-CH_2-1‴), 2.28 (m, 2H, H-4), 2.00–2.07 (m, 2H, H-3), 1.65–0.98 (m, 6H, six methyl protons of xylene), 0.92–0.84 (m, 9H, CH_2-2″, CH_2-3″, CH_2-4″, CH_3-5″). Anal. (C, H, N) calcd: 56.25, 7.29, 7.29; found: 56.39, 7.22, 7.65

Compound ***50***

MS (FAB):M+H^+ peak at *m/z* 398. IR (KBr, cm^{-1}): 3375, 3249 (N–H str. of CONH), 3060 (Ar C–H str.), 2856 (ali C–H str.), 1716 (C=O str.), 1562, 1454 (ali C–H def.), 1323 (S=O str. of SO_2NH, asymmetric), 1155 (S=O str. of SO_2NH, symmetric), 975, 773, 713 (Ar–C–H def.). ^{1}H NMR (300 MHz, CDCl3): δ 12.55 (s, 1H, COOH), 7.31 (s, 1H, H-3′), 7.26 (s, 1H, H-4′), 7.43 (s, 1H, SO_2NH), δ 2.65 (m, 2H, N-CH_2-1‴), 2.28 (m, 2H, H-4), 1.99–2.03 (m, 2H, H-3), 1.65–0.98 (m, 6H, six methyl protons of xylene), 1.39-1.31 (m, 8H, CH_2-2″, CH_2-3″, CH_2-4″, CH_2-5″), δ 0.96-0.90 (m, 3H, CH_3-6″). Anal. (C, H, N) calcd: 57.29, 7.53, 7.03; found: 57.43, 7.52, 6.85

Compound ***51***

MS (FAB):M+H^+ peak at *m/z* 390. IR (KBr, cm^{-1}): 3352, 3249 (N–H str. of CONH), 3056 (Ar C–H str.), 2866 (ali C–H str.), 1726 (C=O str.),1552, 1444 (ali C–H def.), 1317 (S=O str. of SO_2NH, asymmetric), 1153 (S=O str. of SO_2NH, symmetric), 975, 754, 709 (Ar–C–H def.). ^{1}H NMR (300 MHz, CDCl3): δ 12.55 (s, 1H, COOH), 7.31 (s, 1H, H-3′), 7.26 (s, 1H, H-4′), 7.43 (s, 1H, SO_2NH), 2.28 (m, 2H, H-4), 1.99-2.03 (m, 2H, H-3), 1.65–0.98 (m, 6H, six methyl protons of xylene), 7.21-6.99 (m, 5H, phenyl proton). Anal. (C, H, N) calcd: 58.46, 5.64, 7.18; found: 58.63, 5.62, 6.97

Compound ***52***

MS (FAB):M+H^+ peak at *m/z* 435. IR (KBr, cm^{-1}): 3452 (N–H str. of CONH), 3055 (Ar C–H str.), 2925 (ali C–H str.), 1733 (C=O str.), 1602, 1452 (ali C–H def.), 1353 (S=O str. of SO_2NH, asymmetric), 1172 (S=O str. of SO_2NH, symmetric), 956, 798, 707 (Ar–C–H def.). ^{1}H NMR (300 MHz, CDCl3): δ 12.65 (s, 1H, COOH), 8.23-7.9 (m, 4H, nitrobenzyl protons), 7.31 (s, 1H, H-3′), 7.26 (s, 1H, H-4′), 7.43 (s, 1H, SO_2NH), 2.28 (m, 2H, H-4), 1.99-2.03 (m, 2H, H-3), 1.65–0.98 (m, 6H, six methyl protons of xylene). Anal. (C, H, N) calcd: 52.41, 4.83, 9.65; found: 52.63, 4.82, 9.67

Compound ***53***

MS (FAB):M+H^+ peak at *m/z* 418. IR (KBr, cm^{-1}): 3326, 3249 (N–H str. of CONH), 3028 (Ar C–H str.), 2862 (ali C–H str.), 1589, 1456 (ali C–H def.), 1398 (S=O str. of SO_2NH, asymmetric), 1168 (S=O str. of SO_2NH, symmetric), 987, 779, 748 (Ar–C–H def.). ^1H NMR (300 MHz, CDCl3): δ 12.67 (s, 1H, COOH), 7.31 (s, 1H, H-3′), 7.26 (s, 1H, H-4′), 7.43 (s, 1H, SO_2NH), 2.28 (m, 2H, H-4), 1.99-2.03 (m, 2H, H-3), 1.65–0.98 (m, 6H, six methyl protons of xylene), 3.69 (s, 2H, N-CH_2-1″), 2.77 (m, 2H, CH_2-2″). Anal. (C, H, N) calcd: 60.29, 6.22, 6.70; found: 60.45, 6.26, 6.67

Compound ***54***

MS (FAB):M+H^+ peak at *m/z* 342. IR (KBr, cm^{-1}): 3431, 3269 (N–H str. of CONH), 2954 Ar C–H str.), 2867 (ali C–H str.), 1708 (C=O str.), 1562, 1452 (ali C–H def.), 1344 (S=O str. of SO_2NH, asymmetric), 1163 (S=O str. of SO_2NH, symmetric), 968, 792 (Ar–C–H def.). ^1H NMR (300 MHz, CDCl3): δ 12.67 (s, 1H, COOH), 7.31 (s, 1H, H-3′), 7.26 (s, 1H, H-4′), 7.43 (s, 1H, SO_2NH), 2.28 (m, 2H, H-4), 1.99-2.03 (m, 2H, H-3), 1.65–0.98 (m, 6H, six methyl protons of xylene), 3.69 (s, 2H, N-CH_2-1″), 2.77 (m, 2H, CH_2-2″). Anal. (C, H, N) calcd: 52.63, 6.43, 8.19; found: 52.89, 6.55, 7.97

Compound ***55***

MS (FAB):M+H^+ peak at *m/z* 356. IR (KBr, cm^{-1}): 3375, 3257 (N–H str. of CONH), 3066 (Ar C–H str.), 2869 (ali C–H str.), 1712 (C=O str.), 1564, 1458 (ali C–H def.), 1325 (S=O str. of SO_2NH, asymmetric), 1163 (S=O str. of SO_2NH, symmetric), 972, 792, 736 (Ar–C–H def.). ^1H NMR (300 MHz, CDCl3): δ 12.60 (s, 1H, COOH), δ 7.88 (d, 2H, H-2′, H-6′), δ 7.64 (d, 1H, H-3′, H-5′), δ 7.61 (s, 1H, SO_2NH), δ 7.55 (m, 1H, CONH), δ 2.67 (m, 3H, N-CH_3-1‴), δ 3.51 (m, 1H, H-2), δ 2.48 (m, 2H, H_2-4), δ 1.31 (m, 2H, H_2-3), 1.37-0.89 (m, 9H, i-But protons). Anal. (C, H, N) calcd: 53.93, 6.74, 7.86; found: 54.21, 6.75, 7.77

Compound ***56***

MS (FAB):M+H^+ peak at *m/z* 384. IR (KBr, cm^{-1}): 3377, 3257 (N–H str. of CONH), 2958 (Ar C–H str.), 2867 (ali C–H str.), 1712 (C=O str.), 1598 (ali C–H def.), 1330 (S=O str. of SO_2NH, asymmetric), 1161 (S=O str. of SO_2NH, symmetric), 983, 910, 730 (Ar–C–H def.). ^1H NMR (300 MHz, CDCl3): δ 12.62 (s, 1H, COOH), δ 7.88 (dd, J = 14.5, 2H, H-2′, H-6′), δ 7.64 (dd, J = 8.9, 2H, H-3′, H-5′), δ 7.61 (s, 1H, SO_2NH), δ 7.55 (m, 1H, CONH), δ 3.55 (m, 1H, N-CH-1‴), δ 2.48 (m, 2H, H_2-4), δ 1.31 (m, 2H, H_2-3), δ 1.22–1.18 (m, 6H, CH_3-2″, CH_3-3‴). Anal. (C, H, N) calcd: 56.25, 7.29, 7.29; found: 56.61, 7.35, 7.07

Compound ***57***

MS (FAB):M+H^+ peak at *m/z* 398. IR (KBr, cm^{-1}): 3369, 3269 (N–H str. of CONH), 2960 (Ar C–H str.), 2867 (ali C–H str.), 1720 (C=O str.), 1558, 1454 (ali C–H def.), 1336 (S=O str. of SO_2NH, asymmetric), 1163 (S=O str. of SO_2NH, symmetric), 981, 756, 730 (Ar–C–H def.). ^1H NMR (300 MHz, CDCl3): δ 12.56 (s, 1H, COOH), δ 7.88 (d, 2H, H-2′, H-6′), δ 7.64 (d, J = 9.5, 1H, H-3′, H-5′), δ 7.61 (s, 1H, SO_2NH), δ 6.55 (m, 1H, CONH2), δ 3.51 (m, 1H, H-2), δ 2.46 (m, 2H, H_2-4), δ 1.31 (m, 2H, H_2-3), 1.37-0.89 (m, 9H, i-But protons). Anal. (C, H, N) calcd: 57.28, 7.54, 7.03; found: 57.31, 7.61, 6.91

Compound ***58***

MS (FAB):M+H^+ peak at *m/z* 398. IR (KBr, cm^{-1}): 3375, 3265 (N–H str. of CONH), 2954 (Ar C–H str.), 2867 (ali C–H str.), 1718 (C=O str.), 1562, 1461 (ali C–H def.), 1326 (S=O str. of SO_2NH, asymmetric), 1163 (S=O str. of SO_2NH, symmetric), 977, 792, 730 (Ar–C–H def.). ^1H NMR (300 MHz, CDCl3): δ 12.56 (s, 1H, COOH), δ 7.88 (d, 2H, H-2′, H-6′), δ 7.64 (d, 1H, H-3′, H-5′), δ 7.61 (s, 1H, SO_2NH), δ 6.55 (m, 1H, CONH2), δ 3.51 (m, 1H, H-2), δ 2.46 (m, 2H, H_2-4), δ 1.31 (m, 2H, H_2-3), 1.37-0.89 (m, 9H, i-But protons). Anal. (C, H, N) calcd: 57.28, 7.54, 7.03; found: 57.43, 7.52, 6.97

Compound ***59***

MS (FAB):M+H^+ peak at *m/z* 412. IR (KBr, cm^{-1}): 3373, 3255 (N–H str. of CONH), 2952 (Ar C–H str.), 2867 (ali C–H str.), 1712 (C=O str.), 1566, 1463 (ali C–H def.), 1325 (S=O str. of SO_2NH, asymmetric), 1163 (S=O str. of SO_2NH, symmetric), 972, 794, 736 (Ar–C–H def.). ^1H NMR (300 MHz, CDCl3): δ 12.64 (s, 1H, COOH), δ 7.88 (d, 2H, H-2′, H-6′), δ 7.64 (d, 1H, H-3′, H-5′), δ 7.61 (s, 1H, SO_2NH), δ 7.55 (m, 1H, CONH-5), δ 3.51 (m, 1H, H-2), δ 2.72 (m, 2H, N-CH_2-1‴), δ 2.46 (m, 2H, H_2-4), δ 1.31 (m, 2H, H_2-3), 1.19-0.89 (m, 14H, CH-2″, CH_3-3″, CH_3-4″, CH_3-5″). Anal. (C, H, N) calcd: 58.25, 7.77, 6.79; found: 58.41, 7.73, 6.84

Compound ***60***

MS (FAB):M+H^+ peak at *m/z* 424. IR (KBr, cm^{-1}): 3371, 3263 (N–H str. of CONH), 3053 (Ar C–H str.), 2852 (ali C–H str.), 1720 (C=O str.), 1558, 1450 (ali C–H def.), 1336

(S=O str. of SO_2NH, asymmetric), 1163 (S=O str. of SO_2NH, symmetric), 977, 794, 732 (Ar–C–H def.). ^1H NMR (300 MHz, CDCl3): δ 12.61 (s, 1H, COOH), δ 7.88 (dd, J = 12.4, 2H, H-2′, H-6′), δ 7.64 (dd, J = 8.9, 1H, H-3′, H-5′), δ 7.61 (s, 1H, SO_2NH), δ 7.55 (m, 1H, CONH-5), δ 3.51 (m, 1H, H-2), δ 2.72 (m, 2H, N-CH_2-1‴), δ 2.46 (m, 2H, H_2-4), δ 1.31 (m, 2H, H_2-3), 1.01–1.90 (m, 11H, Cyclohexyl protons). Anal. (C, H, N) calcd: 59.43, 7.55, 6.80; found: 59.64, 7.55, 6.57

Compound ***61***

MS (FAB):M+H^+ peak at *m/z* 418. IR (KBr, cm^{-1}): 3355, 3253 (N–H str. of CONH), 3062 (Ar C–H str.), 2867 (ali C–H str.), 1720 (C=O str.), 1550, 1444 (ali C–H def.), 1319 (S=O str. of SO_2NH, asymmetric), 1161 (S=O str. of SO_2NH, symmetric), 973, 794, 752 (Ar–C–H def.). ^1H NMR (300 MHz, CDCl3): δ 12.60 (s, 1H, COOH), δ 7.88 (d, 2H, H-2′, H-6′), δ 7.64 (d, 1H, H-3′, H-5′), δ 7.61 (s, 1H, SO_2NH), δ 7.55 (m, 1H, CONH-5), δ 3.51 (m, 1H, H-2), δ 2.72 (m, 2H, N-CH_2-1‴), δ 2.46 (m, 2H, H_2-4), δ 1.31 (m, 2H, H_2-3). Anal. (C, H, N) calcd: 60.29, 6.22, 6.70; found: 60.47, 6.32, 6.49

Compound ***62***

MS (FAB):M+H^+ peak at *m/z* 432. IR (KBr, cm^{-1}): 3330, 3249 (N–H str. of CONH), 3029 (Ar C–H str.), 2850 (ali C–H str.), 1525, 1458 (ali C–H def.), 1317 (S=O str. of SO_2NH, asymmetric), 1157 (S=O str. of SO_2NH, symmetric), 987,792, 746 (Ar–C–H def.). ^1H NMR (300 MHz, CDCl3): δ 12.59 (s, 1H, COOH), δ 7.88 (d, 2H, H-2′, H-6′), δ 7.64 (d, 1H, H-3′, H-5′), δ 7.61 (s, 1H, SO_2NH), δ 6.55 (m, 1H, CONH2), 3.66 (s, 2H, N-CH_2-1″), δ 3.51 (m, 1H, H-2), δ 2.46 (m, 2H, H_2-4), δ 1.31 (m, 2H, H_2-3), 1.37–0.89 (m, 9H, i-But protons). Anal. (C, H, N) calcd: 61.11, 6.48, 6.48; found: 61.34, 6.43, 6.49

Compound ***63***

MS (FAB):M+H^+ peak at *m/z* 308. IR (KBr, cm^{-1}): 3454 (N–H str. of CONH), 3068 (Ar C–H str.), 2839 (ali C–H str.), 1704 (C=O str.), 1549, 1492 (ali C–H def.), 1326 (S=O str. of SO_2NH, asymmetric), 1159 (S=O str. of SO_2NH, symmetric), 1101 (C-F str), 962, 786, 771 (Ar–C–H def.). ^1H NMR (300 MHz, CDCl3): δ 12.43(s, 1H, COOH), 7.46-7.13 (m, 4H, phenyl protons), 3.69 (m, 1H, H-2), 3.15 (m, 3H, N-CH_3-1″), δ 2.47 (m, 2H, H_2-4), 1.68 (m, 2H, H_2-3). Anal. (C, H, N) calcd: 46.75, 4.87, 9.09; found: 46.98, 4.66, 9.01

Compound ***64***

MS (FAB):M+H^+ peak at *m/z* 360. IR (KBr, cm^{-1}): 3429, 3105 (N–H str. of CONH), 3068 (Ar C–H str.), 2839 (ali C–H str.), 1704 (C=O str.), 1552, 1492 (ali C–H def.), 1336 (S=O str. of SO_2NH, asymmetric), 1151 (S=O str. of SO_2NH, symmetric), 1097 (C-F str.), 989,788, 771 (Ar–C–H def.). ^1H NMR (300 MHz, CDCl3): δ 12.43(s, 1H, COOH), 7.46-7.13 (m, 4H, phenyl protons), 3.69 (m, 1H, H-2), 3.15 (m, 3H, N-CH_3-1″), δ 2.47 (m, 2H, H_2-4), 1.68 (m, 2H, H_2-3), 1.46-1.27 (m, 9H, three methyl groups of t-But). Anal. (C, H, N) calcd: 50.00, 5.83, 7.78; found: 50.34, 5.76, 7.83

Compound ***65***

MS (FAB):M+H^+ peak at *m/z* 425. IR (KBr, cm^{-1}): 3481, 3178 (N–H str. of CONH), 3068 (Ar C–H str.), 2839 (ali C–H str.), 1704 (C=O str.), 1593, 1492 (ali C–H def.), 1342 (S=O str. of SO_2NH, asymmetric), 1180 (S=O str. of SO_2NH, symmetric), 1087 (C-F str.), 962,786, 771 (Ar–C–H def.). ^1H NMR (300 MHz, CDCl3): δ 12.49(s, 1H, COOH), 8.23-7.9 (m, 4H, nitrobenzyl protons), 7.46-7.13 (m, 4H, phenyl protons), 3.69 (m, 1H, H-2), 3.15 (m, 3H, N-CH_3-1″), δ 2.47 (m, 2H, H_2-4), 1.68 (m, 2H, H_2-3), 1.46-1.27 (m, 9H, three methyl groups of t-But). Anal. (C, H, N) calcd: 48.00, 4.94, 9.88; found: 48.24, 4.87, 9.82

Compound ***66***

MS (FAB):M+H^+ peak at *m/z* 408. IR (KBr, cm^{-1}): 3379, 3257 (N–H str. of CONH), 3066 (Ar C–H str.), 2866 (ali C–H str.), 1710 (C=O str.), 1566, 1454 (ali C–H def.), 1338 (S=O str. of SO_2NH, asymmetric), 1159 (S=O str. of SO_2NH, symmetric), 1095 (C-F str.), 973, 746 (Ar–C–H def.). ^1H NMR (300 MHz, CDCl3): δ 12.49(s, 1H, COOH), 8.23-7.9 (m, 4H, nitrobenzyl protons), 7.46-7.13 (m, 4H, phenyl protons), 3.69 (m, 1H, H-2), 3.15 (m, 3H, N-CH_3-1″), δ 2.47 (m, 2H, H_2-4), 1.68 (m, 2H, H_2-3), 1.46-1.27 (m, 9H, three methyl groups of t-But). Anal. (C, H, N) calcd: 55.88, 5.15, 6.86; found: 55.76, 5.33, 6.79

Compound ***67***

MS (FAB):M+H^+ peak at *m/z* 370. IR (KBr, cm^{-1}): 3413, 3141 (N–H str. of CONH), 2977 (Ar C–H str.), 2837 (ali C–H str.), 1718 (C=O str.), 1562, 1454 (ali C–H def.), 1321 (S=O str. of SO_2NH, asymmetric), 1153 (S=O str. of SO_2NH, symmetric), 985, 783 (Ar–C–H def.). ^1H NMR (300 MHz, CDCl3): δ 12.56 (s, 1H, COOH), 7.28 (d, 1H, H-3′), 7.20 (d, J = 2.1, 1H, H-4′), 7.48 (s, 1H, SO_2NH), 6.75 (m, 2H, $CONH_2$), 3.66 (m, 1H, H-2), 2.27 (m, 2H, H-4), 2.02-2.07 (m, 2H, H-3), 1.47- 1.26 (m, 6H, six methyl

protons of xylene). Anal. (C, H, N) calcd: 55.13, 7.03, 7.57; found: 55.54, 7.34, 7.81

Compound ***68***

MS (FAB):M+H$^+$ peak at *m/z* 435. IR (KBr, cm^{-1}): 3463 (N–H str. of CONH), 2975 (Ar C–H str.), 2862 (ali C–H str.), 1720 (C=O str.), 1562, 1460 (ali C–H def.), 1348 (S=O str. of SO_2NH, asymmetric), 1164 (S=O str. of SO_2NH, symmetric), 958, 796, 744 (Ar–C–H def.). ^{1}H NMR (300 MHz, CDCl3): δ 12.65 (s, 1H, COOH), 8.23-7.9 (m, 4H, nitrobenzyl protons), 7.31 (s, 1H, H-3′), 7.26 (s, 1H, H-4′), 7.43 (s, 1H, SO_2NH), 2.28 (m, 2H, H-4), 1.99-2.03 (m, 2H, H-3), 1.65- 0.98 (m, 6H, six methyl protons of xylene). Anal. (C, H, N) calcd: 52.41, 4.83, 9.65; found: 52.63, 4.57, 9.82

Compound ***69***

MS (FAB):M+H$^+$ peak at *m/z* 418. IR (KBr, cm^{-1}): 3326, 3249 (N–H str. of CONH), 3029 (Ar C–H str.), 2862 (ali C–H str.), 1720 (C=O str.), 1583, 1454 (ali C–H def.), 1396 (S=O str. of SO_2NH, asymmetric), 1147 (S=O str. of SO_2NH, symmetric), 989,748 (Ar–C–H def.). ^{1}H NMR (300 MHz, CDCl3): δ 12.66 (s, 1H, COOH), 7.31 (s, 1H, H-3′), 7.26 (s, 1H, H-4′), 7.43 (s, 1H, SO_2NH), 2.28 (m, 2H, H-4), 1.99-2.03 (m, 2H, H-3), 1.65–0.98 (m, 6H, six methyl protons of xylene), 3.69 (s, 2H, N-CH_2-1″), 2.77 (m, 2H, CH_2-2″). Anal. (C, H, N) calcd: 60.29, 6.22, 6.70; found: 60.44, 6.43, 6.59

Anticancer activity

All title compounds (**29–69**) were biologically evaluated for their antitumor activities against EAC cells in Swiss Albino mice. The %TCI of these compounds against the control was determined individually. Mitomycin C was chosen as the universal standard and azaserin and DON were used as the specific standard drugs to compare the activity of the test compounds and these standard drugs showed 100% inhibition. The %TCI of all title compounds (**29–69**) and their logarithmic values (log %TCI) are shown in Table 2.

Molecular modeling study

The 2D-QSAR, kNN-MFA 3D-QSAR and molecular docking studies as well as MD simulation analysis results are as follows:

2D-QSAR study

Total 347 atom-based and whole molecular descriptors were calculated for the 2D-QSAR study. Intercorrelated descriptors were taken into consideration. Highly correlated descriptors (correlation coefficient > 0.60) were grouped together and descriptor with the highest correlation with biological activity was selected from the group. From the remaining 234 descriptors, equations were developed by stepwise forward ($F = 3.0$ for inclusion) and stepwise backward ($F = 2.9$ for exclusion) multiple linear regression analysis using F value as the stepping criteria. The correlation matrix among the selected descriptors used to develop QSAR model was shown in the supplementary materials (Table S1). Calculated values of important descriptors used in QSAR models are shown in the Supplementary materials (Table S2).

Before dividing the dataset into the training and the test sets, regression analysis was performed with the total dataset. Three compounds were found as outliers (Cpd. **55**, **61**, and **66**) as these compounds showed standard residuals more than two units for most of the developed models. At first, the dataset was divided into the test set and the training set by the *Y*-based ranking method. Molecules were first arranged from the highest to the lowest values based on their biological activities and then molecules in the 4th, 8th, 12th, and so on rows were collected. This way eight compounds (**32**, **34**, **36**, **45**, **46**, **53**, **54**, and **68**) were selected for the test set compounds (test set I) whereas the rest 30 was treated as the training set molecules (training set I). Stepwise regression on the training set generated different equations but the number of descriptors was restricted up to five following recommended ratio of 1: 5 for the number of predictor parameters to number of data point (Topliss and Edwards 1979; Eriksson et al. 2003). The best equation was selected on the basis of statistical qualities and predictability as well as overall fitting. It is shown below:

$$\begin{aligned}\mathrm{Log}(\%\mathrm{TCI}) = \; & 2.247(\pm 0.362) - 0.045(\pm 0.015)nCaH \\ & +0.00006(\pm 0.000)f(\mathrm{N})5 - 1.069(\pm 0.214)q11 \\ & +2.149(\pm 0.621)q13 + +0.300(\pm 0.113)\mathrm{B1R_1}\end{aligned} \quad (4)$$

$n = 30$; $R = 0.865$; $R^2 = 0.750$; $R^2_{\mathrm{A}} = 0.698$; $F\ (5,\ 24) = 14.375$; $p < 0.00000$; SEE = 0.137; $R^2_{CV} = 0.515$; PRESS = 0.874; SSY = 1.803; SDEP = 0.174; $S_{\mathrm{PRESS}} = 0.196$; $R^2_{\mathrm{SCR}} = 0.193$; $n' = 8$; $R^2_{\mathrm{Pred}} = 0.689$; $r_{\mathrm{m}}{}^2 = 0.535$

Where n and n' are number of compounds in the training and the test sets respectively. The Eq. (4) explains 69.80% and predicts 51.51% of variances of the biological activity. The external predictability of the model is justified by R^2_{Pred} and $r_{\mathrm{m}}{}^2$ values which are 0.689 and 0.535, respectively. Three atom based descriptors $q11$, $q13$ and $f(\mathrm{N})5$ were found to be important. The $q11$ and $q13$ are Wang-Ford

charges of atom numbers 11 and 13 respectively (Fig. 3). The negative coefficient of $q11$ shows that the lower value of the charge (the negative charge) at the atom number 11 may increase the biological activity. The positive coefficient associated with $q13$ suggests that with the increase in the value of Wang-Ford charge at the atom number 13, the value of the biological activity may be improved, i.e., the negative charge of the atom should be decreased for the increased anticancer activity. As these two atoms are present in the aliphatic chain and are attached to the electronegative atoms/groups like the nitrogen, the carbonyl, etc, it may be concluded that the aliphatic part of the glutamine moiety of these compounds are important for the binding interactions. The $f(N)5$ is the frontier electron density of the atom number 5 present in the aromatic ring of the general structure (Fig. 3). The positive coefficient of $f(N)5$ indicates that the increased nucleophilic attack at the atom number 5 may be favorable for the antitumor activity. Two whole molecular descriptors—*nCaH* (number of unsubstituted aromatic rings) and *B1R1* (Verloop strerimol parameter for R1 substitution) were also found to be important. The negative coefficient associated with *nCaH* suggests that the unsubstituted aromatic rings may not be favorable for anticancer activity, i.e., substitutions at the aromatic rings may play important roles for the better binding in the receptor site. The positive coefficient of *B1R1* suggests that the higher value of this parameter may be conducive to the biological activity.

As only one test set-training set combination may produce biased model, the dataset was also divided by *k*-means cluster analysis (*k*-MCA) technique. Cluster analysis was allowed to split the dataset into four clusters (10, 3, 12 and 13 compounds in those four clusters) and 7 compounds (**35**, **48**, **49**, **53**, **59**, **64**, and **67**) were selected randomly from each cluster to form the test set (test set II). As the number of compounds in the training set raised to 31, six descriptors were allowed to generate models from the training set (training set II). The best found equation is:

$$\begin{aligned}\mathrm{Log}(\%\mathrm{TCI}) = {} & 2.194(\pm 0.327) - 0.044(\pm 0.013)nCaH \\ & + 0.0002(\pm 0.000)f(\mathrm{E})8 \\ & + 0.00007(\pm 0.000)f(\mathrm{N})5 - 1.002(\pm 0.185)\mathrm{q}11 \\ & + 2.287(\pm 0.529)q13 + 0.323(\pm 0.105)B1R_1 \end{aligned} \quad (5)$$

$n = 31$; $R = 0.900$; $R^2 = 0.810$; $R_A{}^2 = 0.762$; $F\ (6,\ 24) = 16.998$; $p < 0.00001$; SEE = 0.123; $R^2{}_{CV} = 0.527$; PRESS = 0.903; SSY = 1.911; SDEP = 0.158; $S_{PRESS} = 0.179$; $R^2{}_{SCR} = 0.179$; $n' = 7$; $R^2{}_{Pred} = 0.693$; $r_m{}^2 = 0.638$.

Table 3 Pharmacological activities of 5-*N*-substituted-2-*N*-(substituted benzenesulphonyl)-L(+) glutamines (**70–122**)

Cpd[a]	R1′	R2′	R3′	R4′	R5′	%TCI
	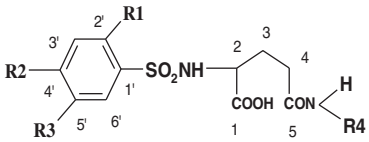					
70	H	NO_2	CH_3	H	*n*-C_4H_9	80.74
71	CH_3	H	H	NO_2	*n*-C_4H_9	89.36
72	Cl	H	H	CH_3	*n*-C_3H_7	83.098
73	H	NO_2	H	H	CH_3	21.74
74	H	NO_2	H	H	C_2H_5	31.34
75	H	NO_2	H	H	*n*-C_3H_7	10.47
76	H	NO_2	H	H	*i*-C_3H_7	41.38
77	H	NO_2	H	H	C_6H_5	32.75
78	H	NO_2	H	H	*n*-C_4H_9	45.45
79	H	NO_2	H	H	*n*-C_6H_{13}	48.86
80	Cl	H	H	CH_3	*i*-C_3H_7	31.69
81	Cl	H	H	CH_3	*n*-C_4H_9	61.97
82	Cl	H	H	CH_3	*i*-C_4H_9	40.00
83	Cl	H	H	CH_3	$C_6H_5CH_2$	56.42
84	H	H	Br	H	*n*-C_4H_9	41.76
85	H	H	Br	H	*n*-C_6H_{13}	48.71
86	H	H	Br	H	*n*-C_3H_7	20.88
87	H	H	Br	H	*i*-C_4H_9	30.76
88	H	H	Br	H	C_6H_5	39.56
89	H	H	H	H	*i*-C_4H_9	12.68
90	H	H	CH_3	H	*i*-C_3H_7	19.13
91	H	H	CH_3	H	*i*-C_4H_9	20.8
92	CH_3	H	H	NO_2	H	19.35
93	CH_3	H	H	NO_2	CH_3	46.77
94	CH_3	H	H	NO_2	C_2H_5	66.19
95	CH_3	H	H	NO_2	*n*-C_3H_7	45.00
96	CH_3	H	H	NO_2	*i*-C_3H_7	42.20
97	CH_3	H	H	NO_2	*i*-C_4H_9	76.29
98	CH_3	H	H	NO_2	C_6H_{11}	71.80
99	CH_3	H	H	NO_2	C_6H_5	33.30
100	CH_3	H	H	NO_2	$C_6H_5CH_2$	70.15
101	CH_3	H	H	NO_2	*n*-C_5H_{11}	78.89
102	CH_3	H	H	NO_2	*n*-C_6H_{13}	67.38
103	H	NO_2	CH_3	H	H	40.32
104	H	NO_2	CH_3	H	CH_3	56.06
105	H	NO_2	CH_3	H	C_2H_5	31.29
106	H	NO_2	CH_3	H	*n*-C_3H_7	32.28
107	H	NO_2	CH_3	H	*n*-C_5H_{11}	61.80
108	H	NO_2	CH_3	H	*n*-C_6H_{13}	65.14
109	H	NO_2	CH_3	H	*i*-C_3H_7	57.97
110	H	NO_2	CH_3	H	*i*-C_4H_9	62.85

The Eq. (5) explains 76.20% and predicts 52.70% of variances of the dependent parameter. The equation has sufficient predictability as justified by R^2_{Pred} and r_m^2 values of 0.693 and 0.638 respectively. However, the best found equation for this test set-training set combination fails to give new descriptor other than *f*(E)8. This is an atom based descriptor that stands for the frontier electron density for electrophilic attack at the atom number 8 which according to the general structure is one of the two oxygens of the sulphonyl group. Oxygen, having two lone pairs of electrons is very much susceptible to electrophilic attack. From the equation, it may be hypothesized that the electrophilic attack on this atom should be increased for the higher activity of these molecules. All regression coefficients used in current 2D-QSAR study are significant at more than 95% confidence interval as shown by *p*- and *t*-values. The *p*-and *t*-values of regression equations were shown in the supplementary materials (Table S3). The observed, calculated, residual, predicted residual and predicted values of these two models (Eq. 4 and Eq. 5) are shown in the supplementary materials (Table S4 and Table S5, respectively).

3D-QSAR kNN-MFA study

The 2D-QSAR model may not be able to show all necessary features for the higher activity. Therefore, a 3D-QSAR study is an essential tool for the prediction of necessary features of these molecules of interest. With a hope to get a realistic 3D-QSAR model, 41 compounds of the current dataset (Table 2) and 53 compounds of earlier published dataset (compound **70–122**) (Samanta et al. 2004) (shown in Table 3) were combined to a set of 94 compounds and these were subjected to KNN-MFA modeling. As the structure of bioactive conformer is unknown, the lowest energy conformation of the optimized structure of the best active compound (compound **59)** was used for alignment of all molecules. The template structure is shown in Fig. 4.

After alignment of these molecules, steric, electrostatic, and hydrophobic charges were calculated. The %TCI activities were directly used as the dependent parameter. The dataset was divided into the training set and the test set by sphere exclusion principle using dissimilarity value 6.5. The test set comprised of 16 molecules (compounds **36**, **37**, **44**, **54**, **57**, **63**, **68**, **70**, **76**, **78**, **81**, **84**, **94**, **106**, **115**, and **116**). The kNN-MFA forward-backward regression ($F = 3.0$ to enter, $F = 2.9$ to remove) provided the best model that is shown below:

kNN method:
Training set size = 78, Test set size = 16
Selected Descriptors:
H_1533, S_1222, S_539, S_1471

Table 3 continued

Cpd[a]	R1′	R2′	R3′	R4′	R5′	%TCI
111	H	NO_2	CH_3	H	C_6H_{11}	38.75
112	H	NO_2	CH_3	H	$C_6H_5CH_2$	28.22
113	H	NO_2	CH_3	H	C_6H_5	47.88
114	H	H	C_2H_5	H	CH_3	34.65
115	H	H	C_2H_5	H	C_2H_5	41.20
116	H	H	C_2H_5	H	*n*-C_3H_7	24.73
117	H	H	C_2H_5	H	*n*-C_4H_9	50.68
118	H	H	C_2H_5	H	*n*-C_5H_{11}	34.06
119	H	H	C_2H_5	H	*n*-C_6H_{13}	70.47
120	H	H	C_2H_5	H	*i*-C_3H_7	54.07
121	H	H	C_2H_5	H	$C_6H_5CH_2$	65.23
122	H	H	C_2H_5	H	C_6H_5	52.36

[a] Compound Number

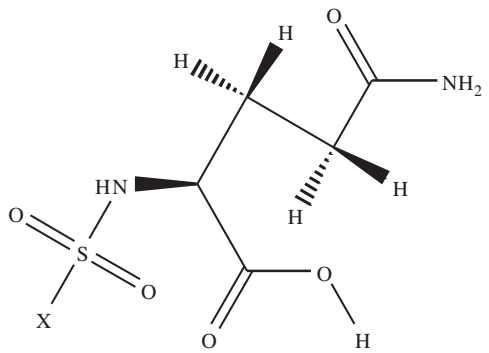

Fig. 4 Template structure for the alignment of structures in kNN-MFA analysis

Statistics:
kNN = 3
Degree of freedom = 73
$q^2 = 0.4923$, ($q^2 = 0.529$, Deleted compounds = **105**, **121**)
q^2_se = 14.6641
Pred$r^2 = 0.1001$ (Pred$r^2 = 0.697$, Deleted compounds = **36**, **97**)
pred_r^2se = 17.4348
Descriptor Range:
H_1533 0.2574 0.2695
S_1222 -0.0210 -0.0145
S_539 -0.0139 -0.0075
S_1471 -0.0031 -0.0024

The kNN-MFA 3D-QSAR model showed the contribution of descriptors H_1533, S_1222, S_539 and S_1471, i.e., hydrophobic interaction field at the lattice point 1533 and the steric interaction fields at lattice points 1222, 539 and 1471 respectively. The model shows q^2 value of 0.492 and Predr^2 = 0.100; Deletion of two compounds (**105, 121**)

from the training set raised the value of q^2 up to 0.529. Deletion of another two compounds (**36**, **97**) from the test set yielded predr^2 0.697. A comparison between the observed and the predicted values in the model showed that the most of the lower active molecules showed the higher values of the deleted residuals. The dataset was directly divided into the higher active (%TCI > 0.50) and lower active (%TCI < 0.50). Compounds were deleted when a higher active compounds was predicted as a lower active compound and vice versa as well as the deleted residual was more than 25 unit. The aligned structures of these molecules as well as descriptors are shown in Fig. 5.

The kNN-MFA 3D-QSAR study showed importance of hydrophobic and steric requirements of these glutamine analogs on the three dimensional space. It is observed that two steric interaction fields were located near to the substituted phenyl ring (Fig. 3) and another steric interaction field was located near the R4 position (Fig. 3). The negative value of all steric interactions at the lattice point 1222, 1471, and 539, respectively (Fig. 3) suggested that the decrease of steric interactions at these positions may be conducive to the higher anticancer activity of these glutamine analogs. Another hydrophobic interaction field was found to be important at the R4 position (Fig. 3). The positive value of the hydrophobic interaction at lattice point 1533 suggested that the hydrophobic interaction at this position may be beneficial for the higher anticancer activity. Therefore, it may be assumed that the lesser bulky substitution with the higher hydrophobicity at the R4 substitution (Fig. 3) may be conducive to the higher anticancer activity of these glutamine analogs.

Molecular docking study

Molecular docking study (Jones et al. 1997) was performed with GOLD software (Astex Technology, Chembridge, UK, 2001). First of all, the original ligand, L-gluatmic acid was docked to the binding site of the same in 3CZD protein to understand how well the docking experiment was performed. At first, the docking was performed setting all amino acids in the binding site rigid. The ligand glutamic acid showed only two hydrogen bonding interactions which did not match with the reported binding interactions of L-glutamic acid at the binding site. Therefore, amino acids in the binding site were rendered flexible and docking was performed again. This time L-glutamic acid showed Goldscore fitness 42.88. The interactions are shown in Fig. 6.

In the docked conformation, the ligand formed hydrogen bonds with Gln285, Ser286, Asn335, Glu381, Asn388 and Tyr249 and forms short contacts with Gln285, Ser286, Asn335, Glu381, Asn388, Tyr414, and Tyr466. No additional interactions were found. Although the binding site and interactions of L-glutamic acid were reported (Jones et al. 1995; Venkatachalam et al. 2003) the same for L-glutamine was not found in the literature. After validating the original ligand, L-glutamine was also docked in the same binding site keeping all parameters same. The best pose showed Goldscore fitness of 40.85. The lower fitness value was due to the less number of hydrogen bond with the binding site amino acids. It showed that hydrogen bond interactions with Glu381, Tyr 249, Tyr414 and Tyr 466 and short interactions with Gln285, Ser286, Asn335, Glu381,

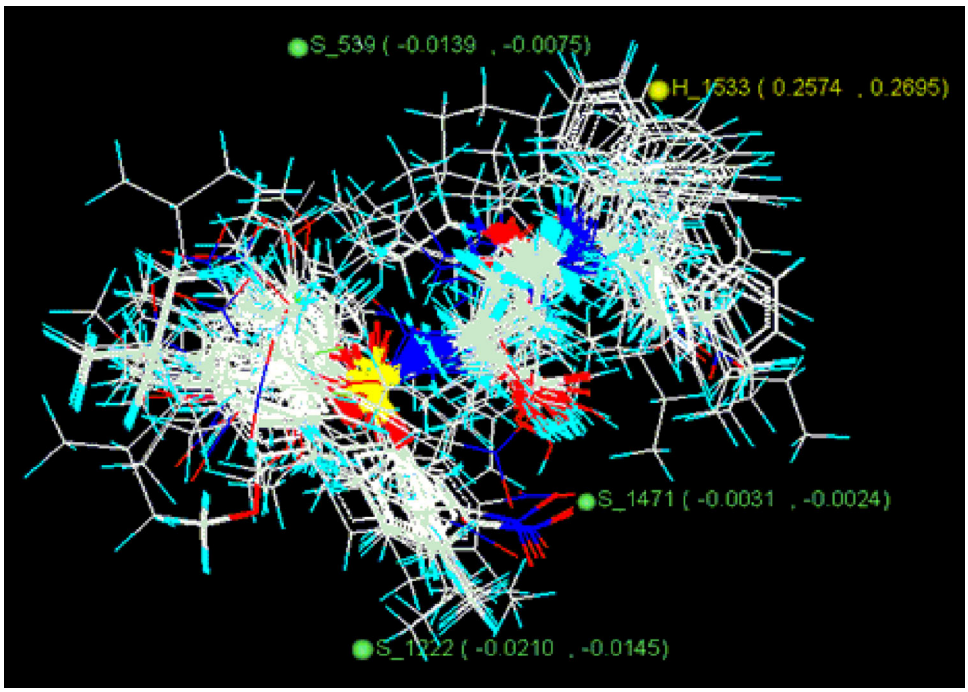

Fig. 5 Graphical representation of the kNN-MFA forward backward regression model

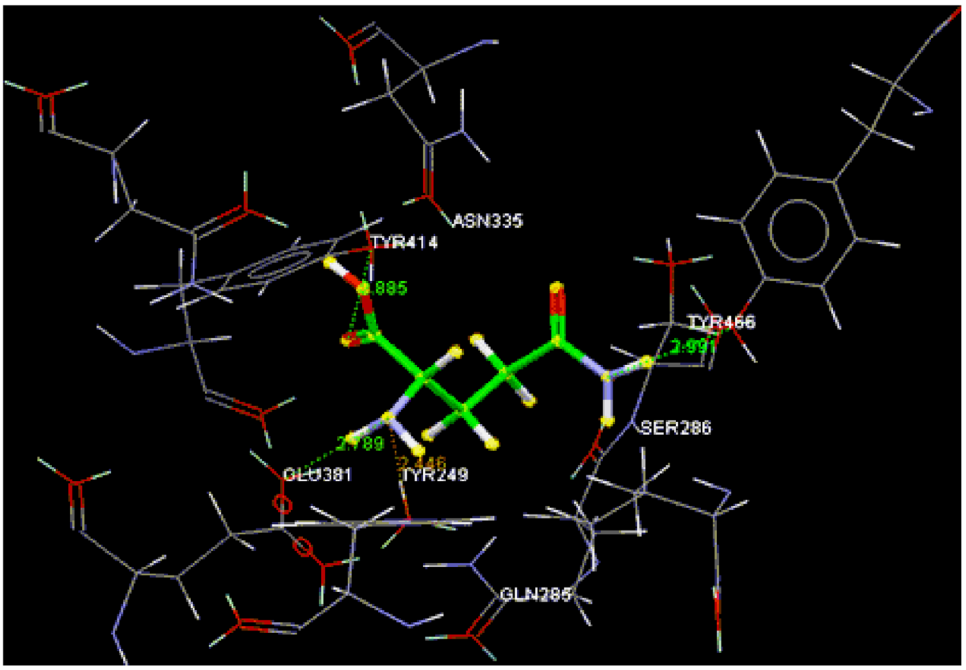

Fig. 6 Best docking pose as well as interactions of L-glutamic acid

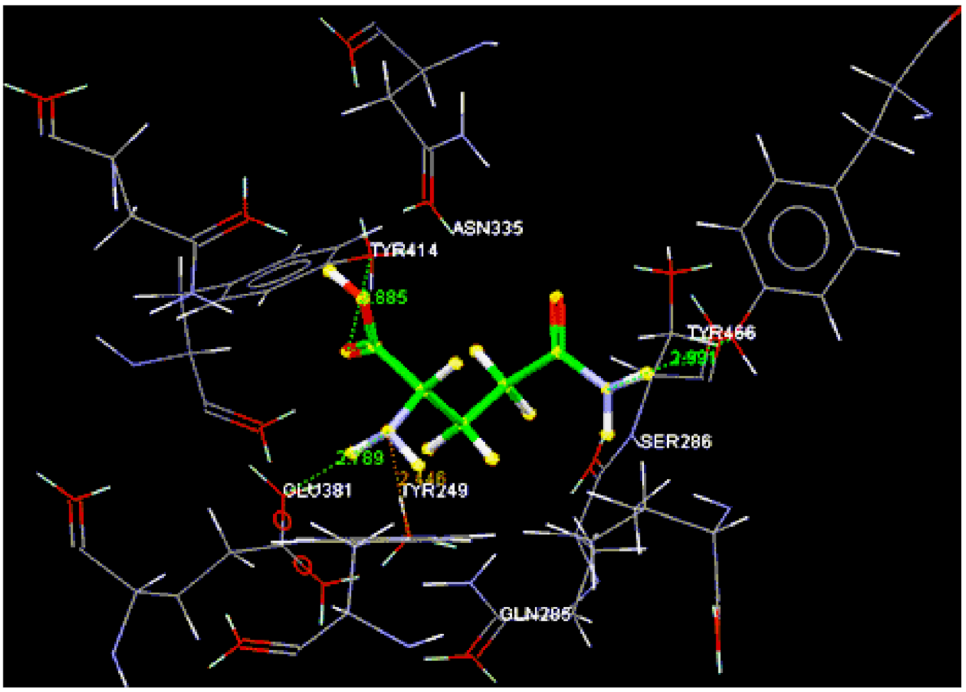

Fig. 7 Best docking pose as well as interactions of L-glutamine

Asn388, Tyr414, and Tyr466. The binding interactions are given in Fig. 7.

The best active compound (compound **59)** was docked similarly. The best pose had Goldscore fitness of 65.82, which was much higher than that of two natural ligands of glutaminase. The best docked conformation is shown in Fig. 8.

The compound **59** was found to form hydrogen bonds with Tyr466, Val 484, Ser286, Tyr414, Asn388, and Glu281. The better Goldscore fitness was due to the higher hydrogen bonding interactions with other amino acids like Gln285, Ser286, Asn335, Glu381, Asn388, Tyr414, Tyr466, and Val484. The lipophilic parts of the compounds like the phenyl ring and its aliphatic substitution like the

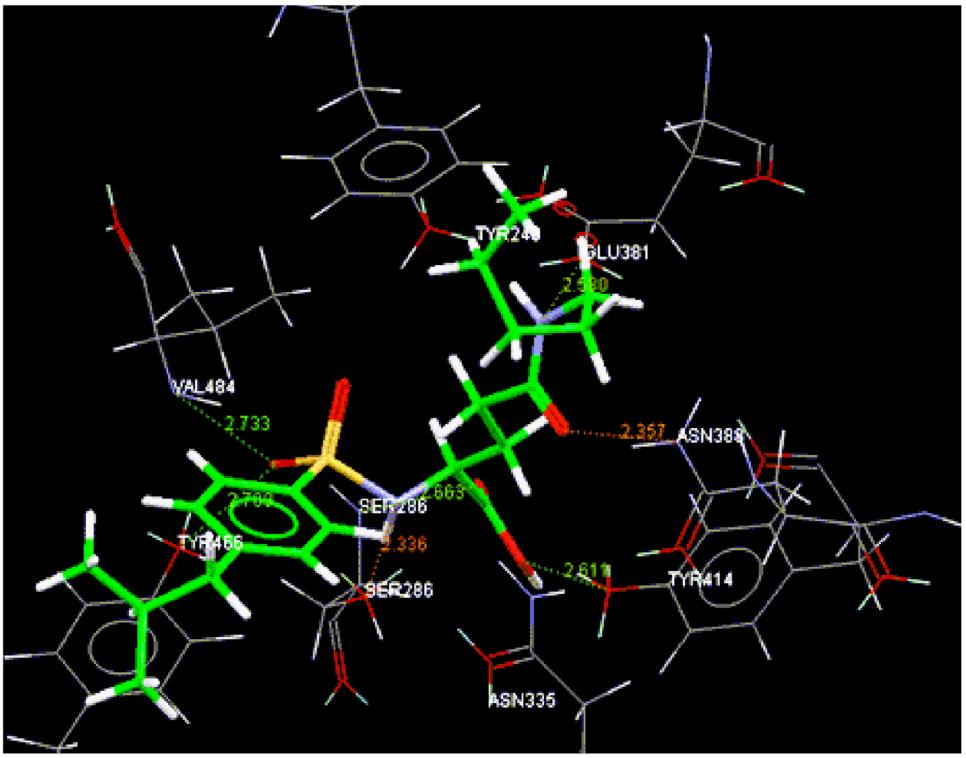

Fig. 8 Best docking pose as well as interactions of Cpd. **59**

isobutyl group were found to form short contacts with amino acid residues of the active site. Hence, it may be concluded that the best active compound may interact with the binding site of L-glutamic acid because of much structural similarity with the ligand and important moieties like the phenyl ring and the sulphonyl group render the better stability in the binding site of the protein.

MD simulation

The geometries of the compound **59** was fully optimized using the density functional theory method with the help of Becke's three parameter hybrid density functional, B3LYP/6–31 G (d, p) using GAUSSIAN3 program (Frisch et al. 2003). This structure was subsequently docked at the glutamic acid binding pocket of 3UNW. The best docked pose showed Goldscore 64.57 which was much higher than that of L-glutamic acid (40.94). The best docked pose (Fig. 8) was found to form hydrogen bond interactions with Tyr249, Ser286, Glu 381, Asn335, and Tyr466. Almost all polar residues showed hydrogen bond acceptor or donor characteristics. The sulfonyl group binds with Tyr466 whereas the adjacent amido group interacts with Asn335. The carboxylic group was found to form hydrogen bond interaction with Ser 286 and Lys289. The amido group attached to the *n*-pentyl residue formed hydrogen bond interaction with Tyr249 and Asn388.

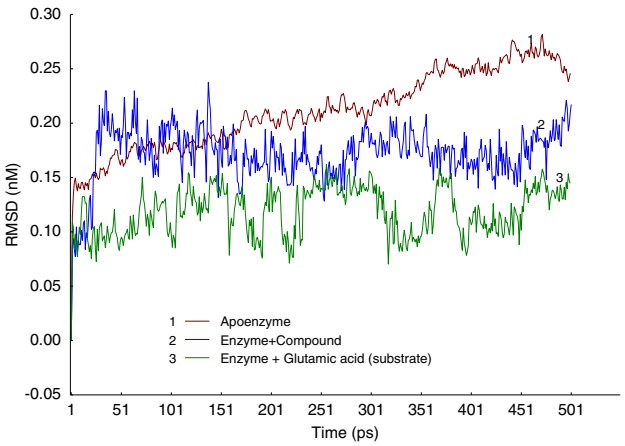

Fig. 9 RMSD plot to investigate the stability of the system

Based on these docking interactions, MD simulations were done on the apo, glutamic acid bound and the compound **59** bound complexes of glutaminase (KGA). These simulations were performed using the GROMACS 4.0.4 program with GROMOS96 43al force field at constant temperature and pressure ensemble. In the MD simulations, all protein atoms were entrapped by a cubic water box of SPC3 water molecules that extended 10 Å from the protein and periodic boundary conditions were utilized in all directions. These systems were balanced with $Na^+$and Cl^- counter ions replacing the solvent molecules. The energy minimization was performed using the steepest descent

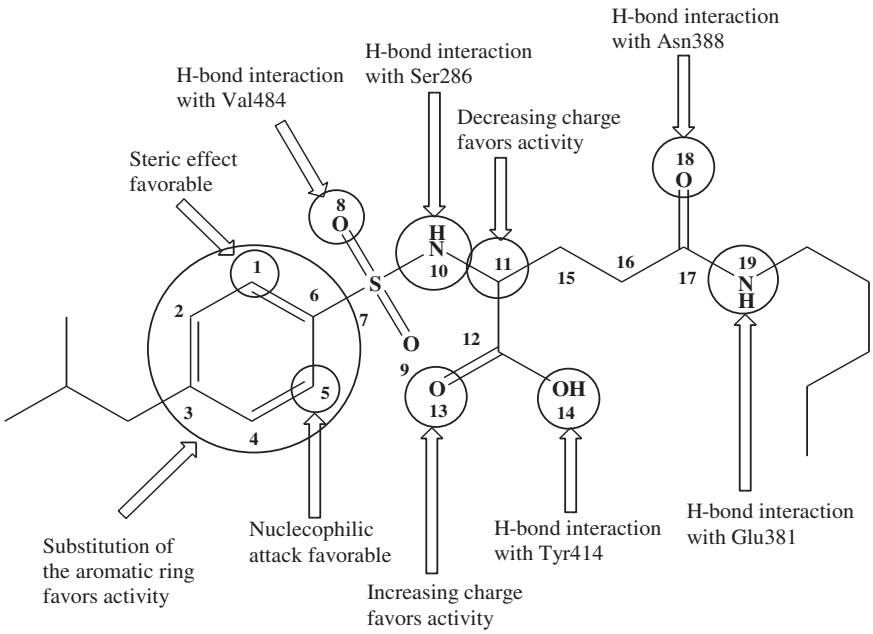

Fig. 10 Structural requirements of glutamine derivatives for better anticancer activity

algorithm for 10000 steps. A 100 ps position restrained MD simulations was performed for every system. It was followed by 500 ps production of MD simulations with a time step of 2 fs constant pressure (1 atm) and temperature (300 K). The electrostatic interactions were calculated by the PME method. All bonds were constrained using LINCS algorithm. The GROMACS topologies for ligands were obtained from PRODRG web server.

The stability of the protein complexes in the MD simulation was also monitored using RMSD calculation with respect to their initial structure. The RMSD vs. time plot is shown in Fig. 9.

The RMSD of glutaminase-L-glutamic acid substrate complex has shown the lowest value compared to all other systems. However, the complex of glutaminase and the best active compound (compound **59**) has shown RMSD value higher than 2.0 Å initially but after 60 ps it maintained consistently below 2.0 Å.

Conclusion

The study carried out here give some important information about the required structural features and possible interactions of 5-*N*-substituted-2-N-(substituted benzenesulphonyl)-L(+) glutamines. The highest antitumor activity was found for the compound **59**. Although there are considerable biological activity variations among these synthesized compounds, lack of structural variations may limit finding of necessary information from a single molecular modeling approach. Therefore, a multiple ligand-based designing methodology by 2D-QSAR and 3D-QSAR analyses as well as molecular docking studies and MD simulation were adopted here separately. The 2D-QSAR study reveals the importance of the sulphonyl group, substitutions of the phenyl ring and charges of the alkyl part of glutamine moiety. The 3D-QSAR study by kNN-MFA mainly focused in the steric and hydrophobic interactions that are close to the substituted phenyl residue and aliphatic/aromatic groups attached to the amido moiety of glutamine residue. The docking study performed with the human kidney type glutaminase (KGA) enzyme depicts that the best active compound **59** may bind to the L-glutamic acid binding site of the protein. Apart from hydrogen bonding interactions formed by electronegative elements like the oxygen and the nitrogen atoms, close contacts formed by steric Van der waals interaction render the better stability in the binding site. The molecular docking study followed by molecular dynamic simulation showed that these compounds may be acting as glutaminase inhibitors through L-glutamic acid binding site of glutaminase enzyme. Atoms and substituents important for the better anticancer activity obtained in molecular modeling studies of these glutamine analogs are presented schematically on the best active compound (compound **59**) in Fig. 10. The current study may help in further tailoring of this series of compounds for obtaining compounds with the better anticancer activity.

Acknowledgements Authors are thankful to the All India Council for Technical Education (AICTE), New Delhi, Council for Scientific and Industrial Research (CSIR), New Delhi and University Grants Commission (UGC), New Delhi for providing financial support. Two authors (AKH and NA) thank Council for Scientific and Industrial Research (CSIR), New Delhi for providing a Senior Research Fellowship (SRF). We are also thankful to the authority of Jadavpur University for providing us the facility required for the work.

Compliance with ethical standards

Conflict of interest The authors declare that they have no competing interests.

References

Adhikari N, Halder AK, Mondal C, Jha T (2013a) Exploring structural requirements of aurone derivatives as antimalarials by validated DFT-based QSAR, HQSAR, and COMFA-COMSIA approach. Med Chem Res 22:6029–6045

Adhikari N, Halder AK, Mondal C, Jha T (2013b) Ligand based validated comparative chemometric modeling and pharmacophore mapping of aurone derivatives as antimalarial agents. Curr Comput Aid Drug Des 9:417–432

Adhikari N, Halder AK, Mondal C, Jha T (2014) Structural findings of quinolone carboxylic acids in cytotoxic, antiviral, and anti-HIV-1 integrase activity through validated comparative molecular modeling studies. Med Chem Res 23:3096–3127

Adhikari N, Halder AK, Saha A, Saha KD, Jha T (2015) Structural findings of phenylindoles as cytotoxic antimitotic agents in human breast cancer cell lines through multiple validated QSAR studies. Toxicol in Vit 29:1392–1404

Adhikari N, Jana D, Halder AK, Mondal C, Maiti MK, Jha T (2012) Chemometric modeling of 5-Phenylthiophenecarboxylic acid derivatives as anti-rheumatic agents. Curr Comput Aid Drug Des 8:182–195

Bhattacharya P, Maity P (2000) Localization of phosphate dependent glutaminase in ascites fluid of ovarian cancer patient. Pathol Oncol Res 6:217–223

Chakraborty D, Maity A, Jain CK, Hazra A, Bharitkar YP, Jha T, Majumder HK, Roychoudhury S, Mondal NB (2015) Cytotoxic potential of dispirooxindolo/acenaphthoquino andrographolide derivatives against MCF-7 cell line. Med Chem Commun 6:702–707

Chakraborty D, Maity A, Jha T, Mondal NB (2014) Spermicidal and contraceptive potential of desgalactotigonin: a prospective alternative of nonoxynol-9. Plos One 9:e107164

Chang WK, Yang KD, Chuang H, Jan JT, Shaio MF (2002) Glutamine protects activated human T cells from apoptosis by up-regulating glutathione and Bcl-2 levels. Clin Immunol 104:151–160

Chatterjee N, Das S, Bose D, Banerjee S, Jha T, Saha KD (2014) Leishmanial lipid suppresses the bacterial endotoxin-induced inflammatory response with attenuation of tissue injury in sepsis. J Leuk Biol. 96:325–336

Chatterjee N, Das S, Bose D, Banerjee S, Jha T, Saha KD (2015) Leishmanial lipid affords protection against oxidative stress induced hepatic injury by regulating inflammatory mediators and confining apoptosis progress. Toxicol Lett 232:499–512

Das S, Chatterjee N, Bose D, Banerjee S, Jha T, Saha KD (2015a) Leishmanial sphingolipid induces apoptosis in Sarcoma 180 cancer cells through regulation of tumour growth via angiogenic switchover. Tumor Biol 36:3109–3118

Das S, Chatterjee N, Bose D, Banerjee S, Jha T, Saha KD (2015b) Antineoplastic impact of leishmanial sphingolipid in tumour growth with regulation of angiogenic event and inflammatory response. Apoptosis 20:869–882

Das S, Chatterjee N, Bose D, Banerjee S, Pal P, Jha T, Saha KD (2014) Lipid isolated from a Leishmania donovani strain reduces Escherichia coli induced sepsis in mice through inhibition of inflammatory responses. Mediat Inflamm 2014, Article number 409694

DeBerardinis R, Lum JJ, Hatzivassiliou G, Thompson CB (2008a) The biology of cancer: metabolic reprogramming fuels cell growth and proliferation. Cell Metabol 7:11–20

DeBerardinis R, Sayed N, Ditsworth D, Thompson CB (2008b) Brick by brick: metabolism and tumor cell growth. Curr Opin Genet Dev 18:54–61

Deswal S, Roy N (2006) Quantitative structure activity relationship studies of aryl heterocycle-based thrombin inhibitors. Eur J Med Chem 41:1339–1346

Dolinska M, Dybel A, Zablocka B, Albrecht J (2003) Glutamine transport in C6 glioma cells shows ASCT2 system characteristics. Neurochem Int 43:501–507

Eriksson L, Jaworska J, Worth AP, Cronin MT, McDowell RM, Gramatica P (2003) Methods for reliability and uncertainty assessment and for applicability evaluations of classification- and regression-based QSARs. Environ Health Perspect 111:1361–1375

Frisch MJ, Trucks GW, Schlegel HB, Scuseria GE, Millam MA, Daniels AD, Kudin KN, Strain MC, Farkas O, Tomasi BJV, Cossi M, Cammi R, Mennucci B, Pomelli C, Adamo C, Clifford S, Ochterski J, Petersson GA, Ayala PY, Cui Q, Morokuma K, Salvador P, Dannenberg JJ, Malick DK, Rabuck AD, Raghavachari K, Foresman JB, Cioslowski J, Ortiz JV, Baboul AG, Sefanov BB, Liu G, Liashenko A, Piskorz P, Komaromi I, Gomperts R, Martin RL, Fox DJ, Keith T, A-Laham MA, Peng CY, Nanayakkara A, Challacombe M, Gill PMW, Johnson B, Chen W, Wong MW, Andes JL, Gonzalez C, Head-Gordon M, Replogle ES, Pople JA (2003) Gaussian 03-Revision B.03. Gaussian Inc, Pittsburgh

Golbraikh A, Tropsha A (2002) Beware of q2! J Mol Graph Model 20:269–276

Gold Ver. 5.0.1, Astex technology, Cambridge, 2011. https://www.ccdc.cam.ac.uk/solutions/csd-discovery/components/gold/

Halder AK, Saha A, Jha T (2013a) Exploring QSAR and pharmacophore mapping of structurally diverse selective matrix metalloproteinase-2 inhibitors. J Pharm Pharmacol 65:1541–1554

Halder AK, Saha A, Jha T (2013b) Exploration of structural and physicochemical requirements and search of virtual hits for aminopeptidase N inhibitors. Mol Divers 17:123–137

Halder AK, Saha A, Saha KD, Jha T (2015) Stepwise development of structure–activity relationship of diverse PARP-1 inhibitors through comparative and validated in silico modeling techniques and molecular dynamics simulation. J Biomol Struct Dynam 33:1756–1779

Hassanein M, Hoeksema MD, Shiota M, Qian J, Harris BK, Chen H, Clark JE, Alborn WE, Eisenberg R, Massion PP (2013) SLC1A5 mediates glutamine transport required for lung cancer cell growth and survival. Clin Cancer Res 19:560–570

Hazra A, Mondal C, Chakraborty D, Halder AK, Bharitkar YP, Mondal SK, Banerjee S, Jha T, Mondal NB (2015) Towards the development of anticancer drugs from andrographolide: semi-synthesis, bioevaluation, QSAR analysis and pharmacokinetic studies. Curr Top Med Chem 15:1013–1026

Hemmateenejad B (2004) Optimal QSAR analysis of the carcinogenic activity of drugs by correlation ranking and genetic algorithm-based PCR. J Chemometr 18:475–485

Hess B, Kutzner C, van der Spoel D, Lindahl E (2008) GRGMACS 4: Algorithms for highly efficient, load balanced, and scalable molecular simulation. J Chem Theo Comput 4:435–447

Huang F, Zhao Y, Zhao J, Wu S, Jiang Y, Ma H, Zhang T (2014) Upregulated SLC1A5 promotes cell growth and survival in colorectal cancer. Int J Clin Exp Pathol 7:6006–6014

Huntress EH, Carten FH (1940) Identification of organic compounds. I. Chlorosulfonic acid as a reagent for the identification of Aryl Halides. J Am Chem Soc 62:511–514

Jones G, Willet P, Glen RC (1995) Molecular recognition of receptor sites using a genetic algorithm with a description of desolvation. J Mol Biol 245:43–53

Jones G, Willet P, Glen RC, Leach AR, Taylor R (1997) Development and validation of a genetic algorithm for flexible docking. J Mol Biol 267:727–748

Klimberg VS, McClellan JL (1996) Claude H. Organ, Jr. Honorary Lectureship. Glutamine, cancer, and its therapy. Am J Surg 172:418–424

Krogsgaard-Larsen P, Liljefors T, Madsen ULF (2002) Text book of drug design & discovery. Taylor & Francis, London

Kumar A, Chowdhury SR, Chakrabarti T, Majumder HK, Jha T, Mukhopadhyay S (2014) A new ellagic acid glycoside and DNA topoisomerase IB inhibitory activity of saponins from Putranjiva roxburghii. Nat. Prod. Commun 9:675–677

Kumar A, Chowdhury SR, Jatte KK, Chakrabarti T, Majumder HK, Jha T, Mukhopadhyay S (2015) Anthocephaline, a new indole alkaloid and cadambine, a potent inhibitor of DNA topoisomerase IB of Leishmania donovani (LdTOP1LS), isolated from Anthocephalus cadamba. Nat Prod Commun 10:297–299

Leach, AR (2001) Molecular modeling principles and applications, 2nd edn. Prentice Hall, England

Lu W, Pelicano H, Huang P (2010) Cancer metabolism: is glutamine sweeter than glucose? Cancer Cell 18:199–200

Marquez J, Sanchez-Jimenez FM, Medina A, Quesada AR, Nunez de Castro I (1989) Nitrogen metabolism in tumor bearing mice. Arch Biochem Biophys 268:667–675

Martin M, Beauvoit B, Voisin PJ, Canoini P, Guerin B, Rigoulet M (1998) Energetic and morphological plasticity of C6 glioma cells grown on 3-D support; effect of transient glutamine deprivation. J Bioenerg Biomembr 30:565–578

Massiere F, Badet-Denisot MA (1998) The mechanism of glutamine-dependent amidotransferases. Cell Mol Life Sci 54:205–222

Matsuno T, Hirai H (1989) Glutamine synthetase and glutaminase activities in various hepatoma cells. Biochem Int 19:219–225

Mondal C, Halder AK, Adhikari N, Jha T (2013) Cholesteryl ester transfer protein inhibitors in coronary heart disease: Validated comparative QSAR modeling of *N*, *N*-disubstituted trifluoro-3-amino-2-propanols. Comp Biol Med 43:1545–1555

Mondal C, Halder AK, Adhikari N, Jha T (2014) Structural findings of cinnolines as anti-schizophrenic PDE10A inhibitors through comparative chemometric modeling. Mol Divers 18:655–671

Mondal C, Halder AK, Adhikari N, Saha A, Saha KD, Gayen S, Jha T (2015) Comparative validated molecular modeling of p53-HDM2 inhibitors as antiproliferative agents. Eur J Med Chem 90:860–875

Nargotra A, Koul S, Sharma S, Khan IA, Kumar A, Thota N, Koul JL, Taneja SC, Qazi GN (2009) Quantitative structure-activity relationship (QSAR) of aryl alkenyl amides/imines for bacterial efflux pump inhibitors. Eur J Med Chem 44:229–238

Newsholme P, Procopio J, Ramos Lima MS, Pithon-Curi TC, Curi R (2003) Glutamine and glutamate--their central role in cell metabolism and function. Cell Biochem Funct 21:1–9

Ogura M, Takarada T, Nakamichi N, Kawagoe H, Sako A, Nakazato R, Yoneda Y (2011) Exacerbated vulnerability to oxidative stress in astrocytic C6 glioma cells with stable overexpression of the glutamine transporter slc38a1. Neurochem Int 58:504–511

Roy PP, Roy K (2008) On some aspects of variable selection for partial least squares regression models. QSAR Comb Sci 27:302–313

Samanta S, Srikanth K, Banerjee S, Debnath B, Gayen S, Jha T (2004) 5-N-Substituted-2-(substituted benzenesulphonyl) glutamines as antitumor agents. Part II: synthesis, biological activity and QSAR study. Bioorg Med Chem 12:1413–1423

Snedecor GW, Cochran WG (1967) Statistical methods. Oxford & IBH, New Delhi

Van Der Spoel D, Lindahl B, Hess B, Groenhof G, Mark AE (2005) GROMACS: Fast, flexible, and free. J Comput Chem 26:1701–1718

Szeliga M, Obara-Michlewska M (2009) Glutamine in neoplastic cells: focus on the expression and roles of glutaminases. Neurochem Int 55:71–75

Tetko IV, Tanchuk VY, Villa AE (2001) Prediction of n-octanol/water partition coefficients from PHYSPROP database using artificial neural networks and E-state indices. J Chem Inf Comput Sci 41:1407–1421

Topliss RP, Edwards P (1979) Chance factors in studies of quantitative structure-activity relationships. J Med Chem 22:1238–1244

Tropsha A (2003) Recent trends in quantitative structure-activity relationships. In: Abraham DJ (ed) Burger's medicinal chemistry and drug discovery, vol 1. 6th edn. Wiley, New York, p 49–75

Tropsha A, Gramatica P, Gomber VK (2003) The Importance of Being Earnest: Validation is the Absolute Essential for Successful Application and Interpretation of QSPR Models. QSAR Comb Sci 22:69–77

Turner A, McGivan JD (2003) Glutaminase isoform expression in cell lines derived from human colorectal adenomas and carcinomas. Biochem J 370:403–408

Venkatachalam CM, Jiang X, Oldfield T, Waldman M (2003) LigandFit: a novel method for the shape-directed rapid docking of ligands to protein active sites. J Mol Graph Model 21:289–307

VLife (2011) QSAR Plus 1.0 is a molecular modelling software of VLife Sciences and Technologies, Pune, India. www.vlifesciences.com

Walker JD, Jaworska J, Comber MH, Schultz TW, Dearden JC (2003) Guidelines for developing and using quantitative structure-activity relationships. Environ Toxicol Chem 22:1653–1665

Wasa M, Bode BP, Abcouwer SF, Collins CL, Tanabe KK, Souba WW (1996) Glutamine as a regulator of DNA and protein biosynthesis in human solid tumor cell lines. Ann Surg 224:189–197

Wasa M, Wang HS, Okada A (2002) Characterization of L-glutamine transport by a human neuroblastoma cell line. Am J Physiol Cell Physiol 282:C1246–C1253

Witte D, Ali N, Carlson N, Younes M (2002) Overexpression of the neutral amino acid transporter ASCT2 in human colorectal adenocarcinoma. Anticancer Res 22:2555–2557

Xie J, Li P, Gao HF, Qian JX, Yuan LY, Wang JJ (2014) Overexpression of SLC38A1 is associated with poorer prognosis in Chinese patients with gastric cancer. BMC Gastroenterol. 14:70

Zalkin H, Smith JL (1998) Enzymes utilizing glutamine as an amide donor. Adv Enzymol Relat Areas Mol Biol 72:87–144